Landsat Radiometry Project
Final Report
2001-2004
NASA Grant NAG5-11351

May 26, 2005

Image Processing Laboratory
South Dakota State University
Brookings, South Dakota

Introduction

This final report summarizes three years of work characterizing the radiometry of the Landsat 4, 5 and 7 Thematic Mappers. It is divided into six sections that are representative of the major areas of effort:

Internal Calibrator Lamp Monitoring
Vicarious Calibration
Relative Gain Analysis
Outgassing
Landsat 4 Absolute Calibration
Landsat 5 Scene Invariant Analysis.

Each section provides a summary overview of the work that has been performed at SDSU. Major results are highlighted. In several cases, references are given to publications that have developed from this work. Several team members contributed to this report: Tim Ruggles, Dave Aaron, Shriharsha Madhavan, Esad Micijevic, Cory Mettler, and Jim Dewald.
At the end of the report is a summary section.

LANDSAT 5 TM IC RESPONSE

Introduction

This section of the final report summarizes the trends observed in the Landsat 5 IC response data. It is currently believed that the changes occurring later in the instrument lifetime, and shown in the following plots, are most likely due to significant changes in one or more components within the IC subsystem, rather than changes to the detector arrays that would affect their response. This hypothesis tends to be supported by the fact that overall image quality, even in bumper mode operation, remains very high.

Review of Data Processing Methodology

The data under consideration here consist of Level 0 calibration data systematically corrected for scan-correlated-shift (SCS) artifacts. Data from Bands 1-4 were also corrected for memory effect (ME) artifacts. Bias-corrected or 'net' integrated pulse values (NPV's) were then extracted for each detector from the artifact-corrected IC data. After extraction, the NPV's were further corrected for temperature effects (Bands 1-4) and outgassing effects (Bands 5 and 7). Finally, a band-level NPV was estimated by averaging the corrected NPV's across all operative detectors (due to an apparent error in the TMACS system that treated detector 4 in Band 2 and detector 3 in Band 5 as 'dead'—as is the case for the Landsat 4 TM—NPV's from these detectors were not included in the calculations).

Lifetime IC Response in LS [001] and LS [100], Bands 1-4

Prior to year 1990, abrupt changes in IC response, on the order of 5% to 10% depending on the band, have been observed in Bands 1-4 of the individual lamp states [001] and [100]. Figures 1a and 1b show these changes observed in the reverse scan data for Band 1. Due to these early discontinuities, they were not seriously considered for future IC-based calibration efforts.

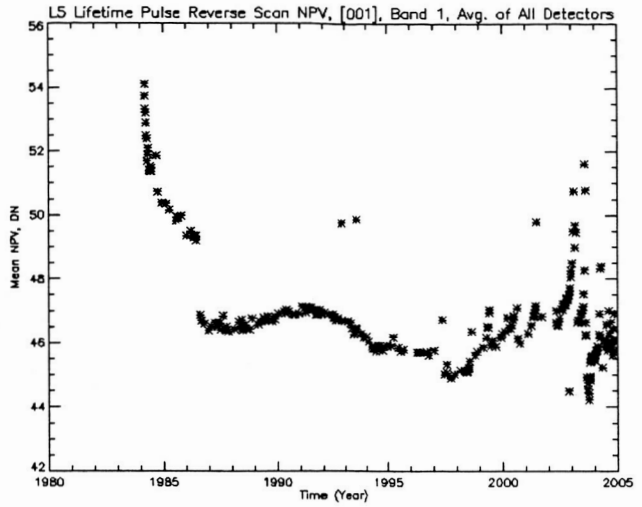

Figure 1a. Band 1 [001] IC Lifetime Response.

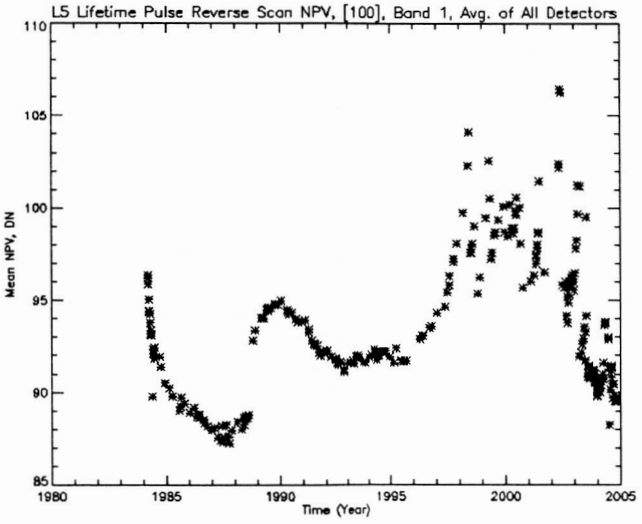

Figure 1b. Band 1 [100] Lifetime IC Response.

Several significant response 'spikes' were also observed for these lamp states, beginning in 1998 for LS [100] and 2000 for LS [001], indicating the occurrence of intermittent 'flare-ups' in the lamps. These changes have continued to occur after the transition to bumper mode operation in early 2002, as shown in the Band 1 plots of Figures 2a and 2b. For LS [001], the maximum variation observed in this period is on the order of 10% to 16%, depending on the band. There are periods of relatively stable response prior to and following these spikes. There also appears to be a general decrease in response, on the order of 10% to 16%, observed in LS [100] during this same period.

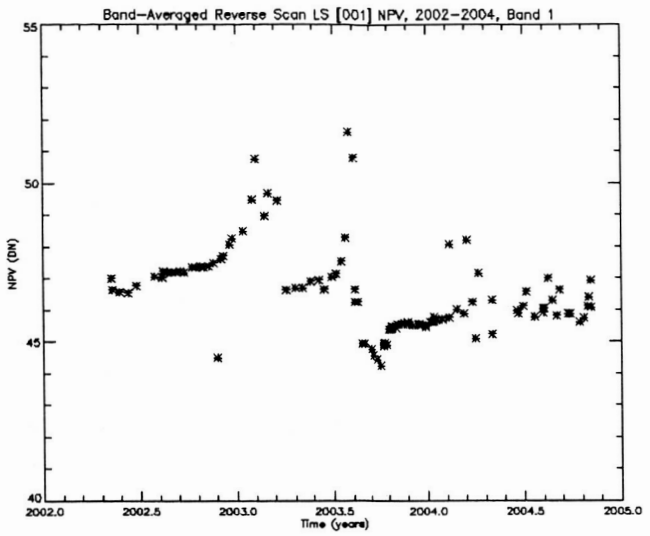

Figure 2a. Band 1 [001] Bumper Mode IC Response. Two spikes in response occurred in 2003; the larger spike in mid-2003 was on the order of 10-15% (depending on band). Overall lamp output appeared to be relatively stable prior to and following these spikes. Smaller response spikes may have occurred in early 2004, followed by even smaller spikes later on.

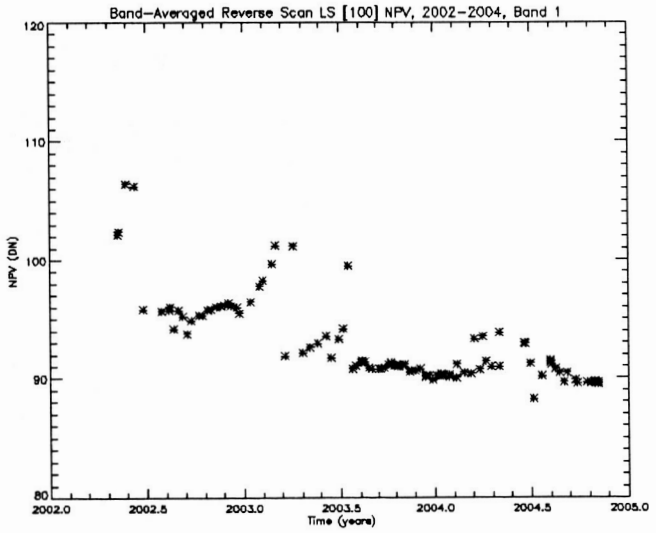

Figure 2b. Band 1 [100] Bumper Mode IC Response. An abrupt change in response was observed in mid 2002, following the transition to bumper mode operation. In addition to apparent response spikes occurring during early to mid 2003, there appeared to be a general decrease in response on the order of 10% to 15% during this period. Note the periods of relatively stable response from mid 2002 to early 2003 and mid 2003 after each response spike; another period of stable response was observed after a slight response dip in mid-2004.

Lifetime IC Response in LS[001] and LS[100], Bands 5 and 7

Figures 3a and 3b show the lifetime IC response in Band 5 for LS [001] and LS [100], respectively.

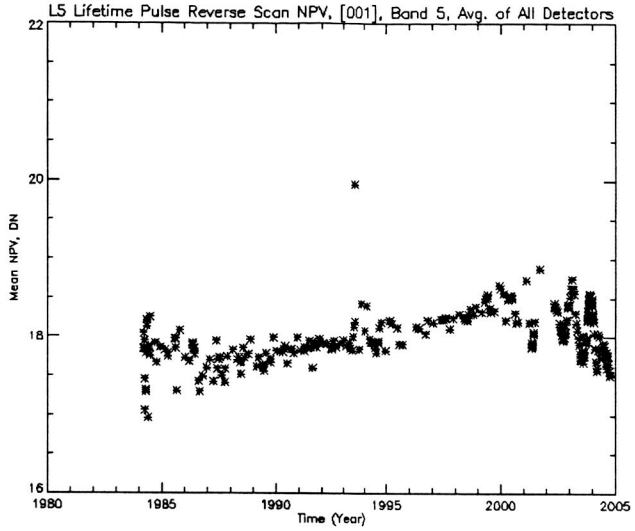

Figure 3a. Band 5 [001] Lifetime IC Response.

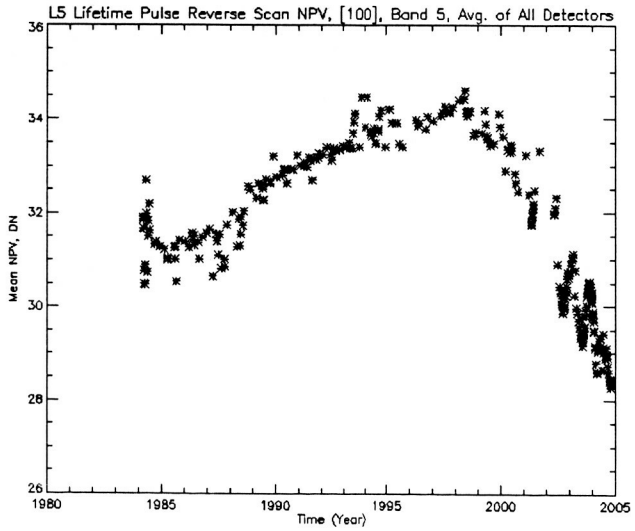

Figure 3b. Band 5 [100] Lifetime IC Response.

Several things are noticeable from these plots. First, the discontinuities in Band 1-4 responses observed in 1986 and 1988 cannot be readily observed in these bands.

Second, changes in IC response can be observed beginning in 1998 for LS [100] and 2000 for LS [001] that correlate with the observed changes in Bands 1-4. However, the character of the response change appears to be radically different. The response spikes observed in Bands 1-4 cannot be easily observed here; rather, the response change appears to be a steady decrease on the order of ~5.5% in LS [001] and ~8% in LS [100]. Finally, it is apparent that the current Band 5 outgassing correction is not effective, as indicated by the oscillations in response occurring from 2002 onwards. Figures 4a and 4b show the post-bumper mode changes in response in greater detail.

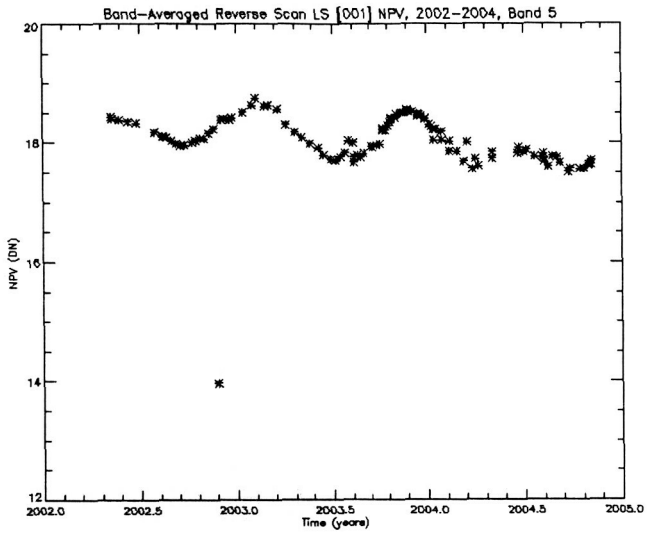

Figure 4a. Band 5 [001] Bumper Mode IC Response. Superimposed on the variation in response due to insufficiently corrected outgassing effects is an approximately 5.5% overall decrease in response.

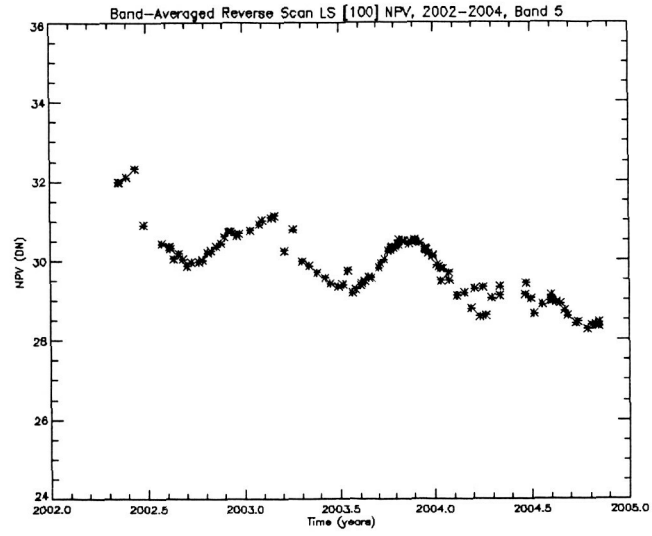

Figure 4b. Band 5 [100] Bumper Mode IC Response. There is an approximately 8% decrease in overall IC response superimposed on the variation due to insufficiently corrected outgassing effects.

Lifetime IC Response in LS [010], Bands 1-4

The remaining lamp state, [010], exhibited no apparent discontinuities in response in any reflective band prior to year 2000, as can be seen from the Band 1 plot shown in Figure 5. A reasonably simple 'normalized' model was derived from these data sets, which consisted of an early exponential decrease in response (believed to be due to outgassing from the spectral filters) followed by a linear increase in response. In general, these models were able to account for up to 95% of the observed variability in response; however, a second-order long period oscillatory effect could not be accounted for. The later linear increase was judged to be a 'false' effect, more likely due to changes in various components within the IC subsystem rather than changes to the detectors themselves; this hypothesis was supported by the fact that no such response trend had been observed in the vicarious calibration data, which are acquired through a different optical pathway within the instrument. As a result, the linear term from the normalized models was removed, leading to a normalized 'exponential-only' model to characterize the IC response. A lifetime calibration model for each band was obtained by scaling the exponential-only models to the estimated gain obtained in a cross-calibration measurement with the Landsat 7 ETM+ performed June 1-4, 1999. The models are currently implemented in a lookup table used by the NLAPS processing system.

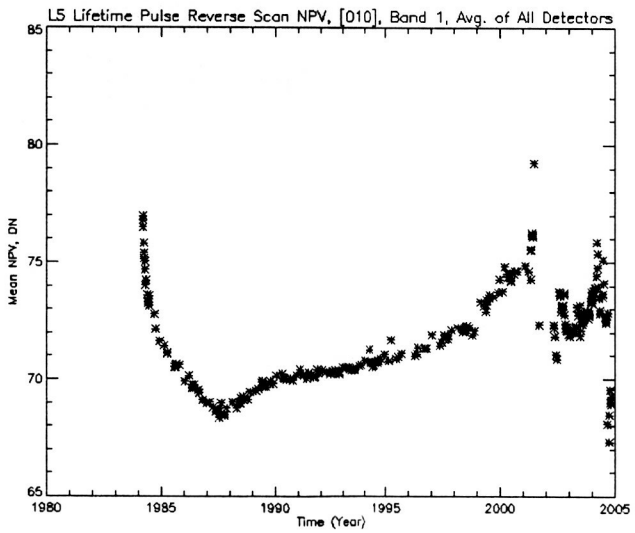

Figure 5. Band 1 [010] Lifetime IC Response.

Following an apparent increase in the response beginning in 2000, a significant response spike was observed to occur in mid to late 2001; this post-2000 behavior effectively rendered extension of the calibration model beyond 2000 impossible. Following this spike, the response tended to stabilize in the period from mid 2002 to early 2003. The response changed slightly in mid 2003 (corresponding to the changes in response affecting the other lamps), and resumed a fairly stable response pattern until early to mid 2004, when two response spikes appear to have occurred (the poor sampling

of data during this period makes a definite statement more difficult). Later in 2004, a decrease in response on the order of 6% to 8% was observed (depending on band), with an indication that the response was returning to a previous level. The character of the post-bumper mode response can be seen more clearly in the expanded plot shown in Figure 6.

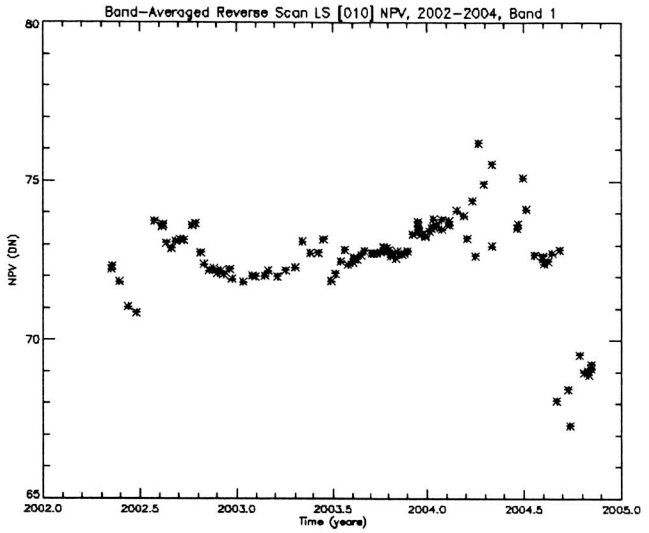

Figure 6. Band 1 [010] Bumper Mode IC Response. There is an apparent discontinuity in response beginning in mid 2002, after the transition to bumper mode. The response tended to remain fairly stable until mid 2003, when the same phenomenon that caused significant spikes affecting LS [001] and LS [100] caused a slight decrease. The response stabilized after this 'upset' event until early to mid 2004, when two response spikes may have occurred. These spikes were followed by a short period of relative stability and a significant drop in response observed later in 2004.

Lifetime IC Response in LS [010], Bands 5 and 7

Figures 7 and 8 show the Band 5 lifetime and post bumper-mode IC responses, respectively. Interestingly, the response maximum in late 2003 is approximately 1 DN greater than the level observed for the early 2003 maximum. There does not appear to be any event in the Band 5 responses in the other lamp states, or in the Band 1-4 responses in this lamp state, that might account for this change; it is possible that this may be an artifact introduced by the outgassing correction. Due to the relatively sparse sampling, it is difficult to estimate the decrease in response for the scenes acquired later in 2004; for Band 7, it is on the order of 3%.

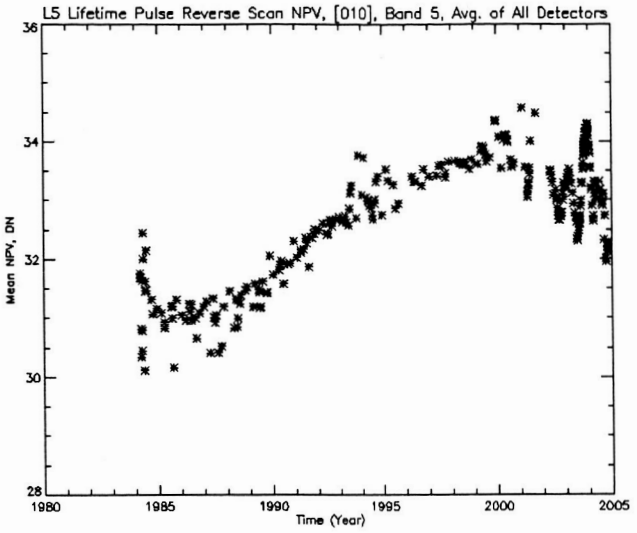

Figure 7. Band 5 [010] Lifetime IC Response.

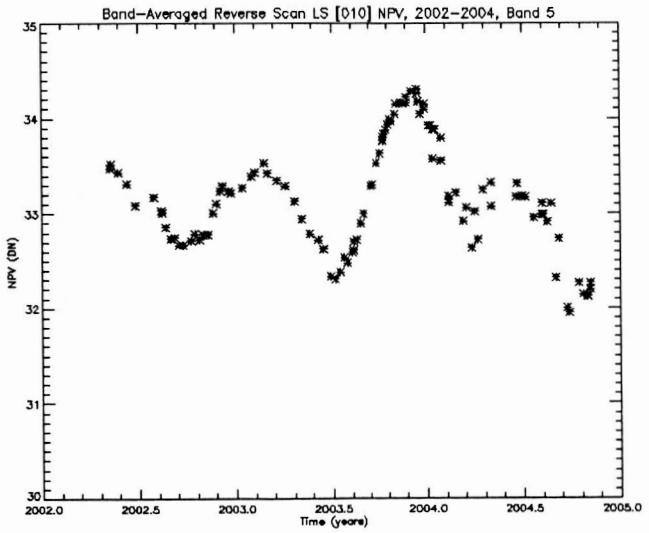

Figure 8. Band 5 [010] Bumper Mode IC Response. The outgassing maxima for 2002 and early 2003 are at a comparable DN level; the maximum for the cycle later in 2003 is approximately one count higher. Due to the poor sampling throughout 2004, it is somewhat difficult to estimate the overall change in response for the scenes acquired later in 2004; it would appear to be less than the Band 7 estimate of approximately 3%.

Conclusion

Since the later-lifetime (post-1998) changes in IC response do not appear to have any correlation to image or vicarious calibration data, it seems reasonable to conclude that they are due to changes occurring only within the IC subsystem. These changes suggest the beginning stages of failure either in the lamps themselves, or in the fiber optic cables and/or lenses that direct the lamp outputs to the focal planes. A cursory

examination of post-2002 telemetry data [1] suggests that at least through 2003, there did not appear to be significant changes in the lamp currents that would demonstrate lamp failure. It is possible that the lamp filaments are experiencing accelerated degradation, leading to random spikes/drops in their overall output as bits of the filament burn off. As LS [100]'s output is not attenuated, it would seem reasonable that any changes in its output would be easiest to detect; the attenuated nature of LS [001] and [010] could be 'masking' significant changes to some extent. A more thorough sampling of IC data throughout the lifetime, as would be provided by the upcoming TM Image Assessment System (TMIAS) could help to answer some of these questions.

References

1. http://landsat-cal.gsfc.nasa.gov/ias_web/L5_trending.html . A valid user 'ID' and password is required to access the site. I used 'truggles' and 'tr_LPSO' for the username and password, respectively.

Vicarious Calibration

2002-2004

The radiometric calibration phase of SDSU's Landsat activities was a continuation of the work begun by Steve Schiller from the Physics Department. Beginning in 2002, this work was transitioned to a new team led by David Aaron (also in the SDSU PhysicsDepartment). The primary goal of the 2002-4 phase was to maintain the ground based vicarious calibration assessment of Landsat 5 and 7. The secondary goal was to fully transition the vicarious calibration activities to the new team. The final goal was to 'productionize' data collection and analysis procedures and processes.

The vicarious calibrations were successfully accomplished; however, the recent cool cloudy summers in South Dakota minimized the number of clean 'high confidence' data collections. The project has been successfully transitioned to the new team at SDSU. This transition was accomplished with the kind assistance of Steve Schiller, the Goddard team, Kurt Thome's University of Arizona Remote Sensing Group, and the JACIE group from Stennis Space Center. Finally, excellent strides were made in reworking our procedures, instrumentation set, and especially in upgrading the analysis software. Protocols now have the team routinely doing data verification in less than 24 hours of a collection and, while not yet routine, pilot studies have verified a process capability of less than 1 week for full data analysis.

Activities: For 2002-2004 data collections were attempted for most overpasses during the summer months (June thru mid September) for both Landsat 5 and 7. Data collection activities centered around Brookings South Dakota. In 2003 an attempt was made to expand the data collection to a crop site (corn). However, a pullback to the traditional 'scene center' grass site was made as a response to the Landsat 7 SLC malfunction.

Personnel from the radiometry team were included on trips to Goddard Space Center and NASA headquarters for technical interchange meetings. Also David Aaron and Gyanesh Chander (EROS Data Center), traveled to the University of Arizona for instrument calibration/repair and participated in a Ivanpah Playa data collection. Numerous meetings and joint data collections (primarily for high resolution commercial satellite assessment) with Stennis Space Center personnel were also undertaken.

Radiometry:

Data Sites and Equipment:

Grass Site:

The primary ground site used for radiometry in this study is within an area located in southeast Brookings that has been previously designated as 'the 3M site'. The site is located within a field consisting of rough grasses and weeds. The site and the surrounding 40+ acres contain the same vegetative mix to minimize adjacency effects. In previous years, radiometric irregularities due to uneven live vegetation and clumped dead vegetation have seriously complicated data analysis. To minimize this problem, an area within the site approximately 250m EW by 150m NS in 2002 and slightly reduced 2003-4 was predefined. To simplify MTF measurements (for related high resolution satellite work) the area is rotated from true north by 6 degrees. Maximum elevation change is 4.9 m (see contour map). The site location (courtesy Stennis GRIT):

Northwest corner at: Lat: 44°17'31.12"N Long: 96°45'59.34"W
Southeast corner at: Lat: 44°17'25.15"N Long: 96°45'48.70"W

This area was routinely maintained by either a mowing service (2002) or by members of the calibration group. The 'grass' was nominally kept mowed to a height of about 10cm using tractor-powered 6-foot rotary mowers. In 2002 and for the August thru October 2004 dates, the east 80m and the west 20m of the site was mowed using a 'lawn mower' and the clippings were bagged and removed. These areas were used for pulse MTF ('blue tarp') and mirror MTF studies for ancillary high resolution satellite projects. Within the center section the clippings were not collected. For safety, within the tarp areas an attempt was made to fill various in-ground holes (gopher/badger dens).

To better maintain data reproducibility and facilitate setup, a system of in-ground markers (30 cm iron spikes labeled with plastic 'ear tags') was established and surveyed (courtesy of the Stennis GRIT). The markers were deployed to define the site boundaries and the location of select equipment and targets. These markers were driven flush with the ground (recall the site must be mowed). If a stake location was 'lost', the stake was easily re-located using a standard metal detector. A basic contour map of the site was developed in 2003. The availability of the site, owned by the Brookings division of the 3M Corporation, is gratefully acknowledged.

Instrumentation:

The basic electronic/optical instrumentation used by the SDSU group has been previously described. The primary equipment base includes:

- Automated SunPhotometers designed and built by the University of Arizona's Electrical and Computer Engineering Department.
    - Unit 08: A good, solid instrument which has been in use for many years. It generally works well but is beginning to show its age (occasional heater malfunction and tends to lose tracking in moderate cloud cover). Always deployed on CEH rooftop (about 2 miles from site).
    - Unit 30: A new '2000' series sunphotometer received in April of 2004. More compact and tracks well even during moderate cloud cover. The unit is typically field deployed using a generator as a power source.
    - Unit 20: This was borrowed from UA for part of the 2003 season (when unit 08 was experiencing problems)
- A Fieldspec model FR spectro-radiometer (ASD unit 638). Work in 2002 was under calibration 8 and 2003-4 was under calibration 10.
    - Backup was generally provided courtesy of EROS Data Center and their unit 6219. The backup was never 'required'; however, on some collections cross validation was done using unit 6219.
- An 18 inch 99% reflectance Spectralon^{tm} panel (Labsphere) is used for 'white reference' data. BRDF was characterized by the University of Arizona's remote sensing group.
    - For backup, new 12" 99% and 12" 75% reflectance panels were purchased

- Several MFR Shadowband units (by Yankee Environmental Systems). Generally one is deployed at the rooftop site and another is deployed at the grass site
- RTRM (Real time reference monitor). A new instrument was designed and built based around an Ocean Pacific compact spectrometer. This unit provides a relative but continuous monitor of radiance as reflected from a 75% spectralon panel. This data is used to then sort and interpolate the actual ASD ground data.
- Ancillary support instrumentation for weather, sky path radiance, etc.

In addition to the above, a computer with a backup RAID unit was procured and an archiving plan for field data was established. Data is also routinely backed-up to an on-campus mainframe archival system.

Data collection Protocols:

For the ASD grass data, the 8° optic was mounted on an adjustable pole and held at a nominal height 1.5 m above the surface (at normal to surface). This produces a sampling area of about 20 cm in diameter. For the white reference data, the panel is leveled and the seam is aligned with the sun to eliminate shadowing. The ASD optic is held about 50cm above the panel. Grass data is taken while walking on NS transects of the site. Generally from 8 to 10 'rows' are collected, interspersing white reference panel data between each pair of rows.

Procedure:

-Warm up instrument for 15 minutes.

- Collect 'white reference' data (generally three sets)

-While walking, collect grass data down (south) one row and up (north) the next.

ASD setting:

Set to 20 spectra/file; 10 files per save

(Typical Folders: Aug23\SDSU3M)

This parameter set results in 40 or 50 files per row (depending on walk speed).

-collect another white reference data series

-walk/collect on the next grass rows, down and back

-continue

A complete collection over the site requires about ½ hour and produces 500-600 files. If there are 'scattered' clouds, collection is generally interrupted any time a cloud obstructs the sun. During data collection, a 'walk sheet' is generated (by hand), which attempts to describe what was happening and when (note that there may be minor discrepancies in file numbers on this sheet. Usually they are quite obvious).

The 10 band sunphotometer (ASR) data is collected every minute from sunrise to sunset. Data collected with unit 08 is from the rooftop of a building (elevation 518m above sea level versus the site's elevation of 505m). Starting in 2004, the new ASR 2000 (unit 30) is generally deployed at the north edge of the site. Shadowband MFR (for evaluating diffuse to global radiance ratio) units are always deployed at rooftop and sometimes at the north edge of the field. V_0 values (zero air mass DN) for the sunphotometers are obtained and monitored by deploying the units on 'clean' days. For all units, stability has been excellent (generally <1% change per year for ASR 30, over 3 years for ASR 08).

Weather data is primarily from the Brookings municipal airport (~2km from site, elevation 502m). In addition, weather satellite imagery (GOES) is downloaded and archived for reference purposes.

Two to three, blue 'corner marker' tarps are deployed just outside of the NW and the SE boundary to assist in clearly delineating the site area on the imagery.

Data Processing:
The raw grass spectral data is processed using a data reduction program which produces time and white reference panel BRDF corrected reflectances averaged over the entire site. This is a MATLAB based program that was developed and refined by SDSU personnel (2001-2003). The raw data is stored in the archive as ASD_Level_0 and the reflectance data is stored as the ASD_Level_1.

Sunphotometer data is reduced via the Langley analysis method. Again a MATLAB based program is used (developed 2002-2004). A front end is nearing completion that will semi-automatically 'remove' clouds (simply eliminating data lines where the sun was obscured by scattered clouds).

The reduced sunphotometer data is passed to another program (presently an Excel spreadsheet, but will be folded into the MATLAB Langley analysis) which removes Rayleigh scattering and produces extinction coefficients for the 10 sunphotometer wavelengths.

With the calibration activity being transitioned to new personnel, the group's experience in MODTRAN modeling was severely degraded. Consequently, the group would like to thank and commend Kurt Thome and the Remote Sensing Group of the University of Arizona for their work in doing the modeling for the 2001-2003 data collections. The project phase simply could not have been continued without their assistance.
Starting in late 2003 with full implementation in 2004, the SDSU group once again has atmospheric analysis capability. Primary analysis is under MODTRAN 4, with supplementary analysis (within an experiment to produce a very short turnaround, moderate accuracy model) using an Excel spreadsheet based model from NREL.

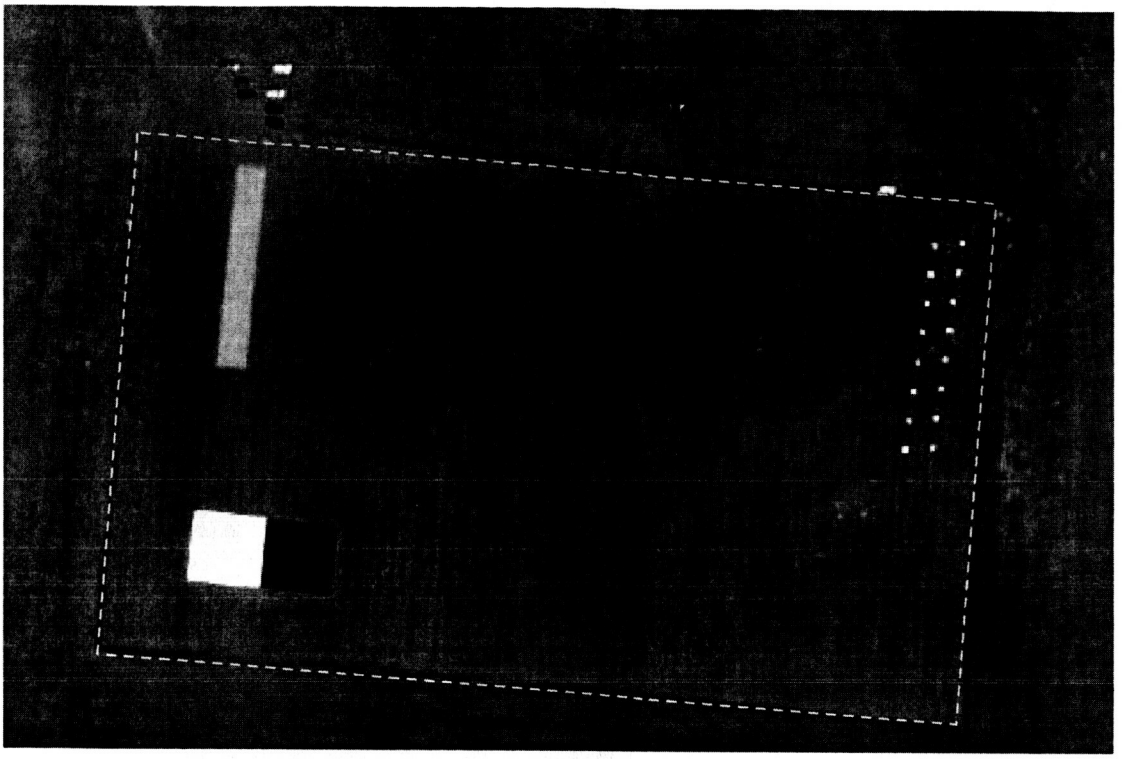

Figure 1: A typical view of the SDSU grass site area from Sept 7, 2002 (Quickbird imagery). The area within the dotted lines is approximately 250 m east-west by 150 m north-south and is regularly mowed. Note the discrete targets shown are not generally deployed for Landsat acquisitions.

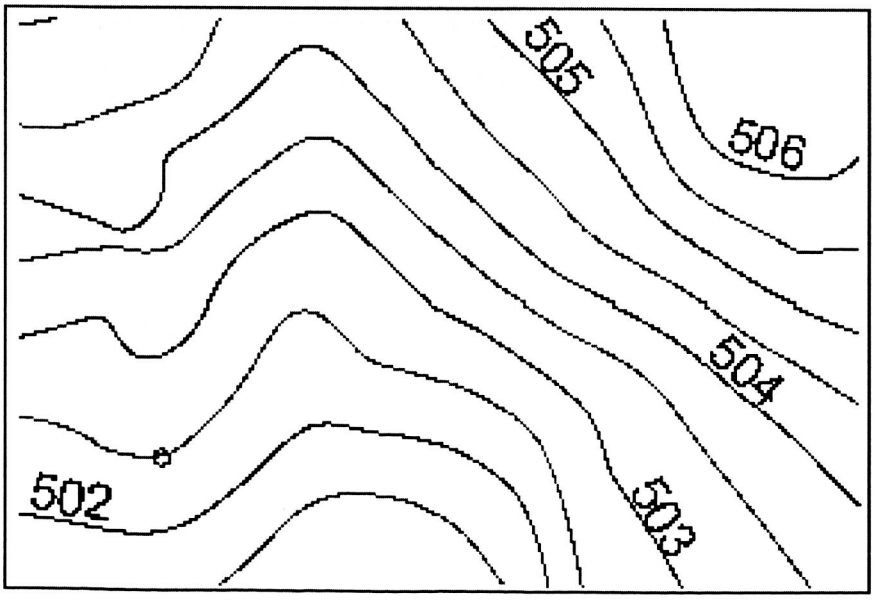

Figure 2: Site elevations in meters as measured by SSC GRIT. Scale is approximately equivalent to that shown in figure 1.

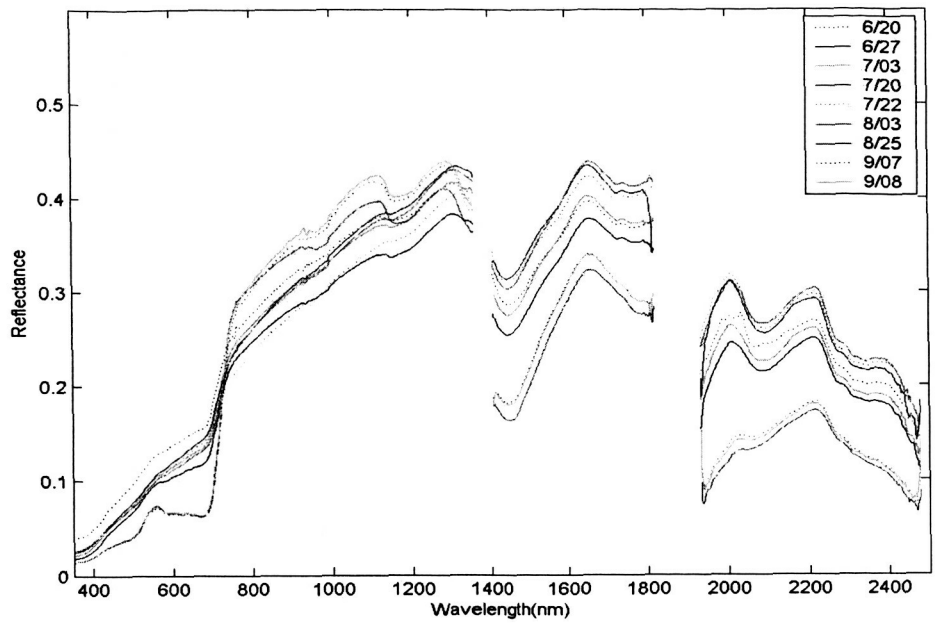

Figure 3: Average grass hyperspectral reflectances for select dates in 2002. Note that the major water bands have been removed for clarity.

Summary of SDSU Landsat Data Collects:

Summer 2002

Generally 12:04 & 12:05pmCDT overpass

June 20: Landsat 7 & EO-1

Good collect
Light Cirrus Wisps
Deployed Blue MTF tarps (Ikonos width)
Ground ASD Reflectance Uniformity of: 6.2% 450-1350nm
6.9% 1410-1800nm
10% 1940-2470nm

July 22: Landsat 7; EO-1 and Ikonos

Good collect
Good weather, slightly hazy
Stennis Tarps Deployed
Blue MTF deployed
Mirrors Deployed
Also deployed (N of maintained area), Plant Science '4 reflectance tarps'
ASD data from Stennis also
Also extensive Cropscan II data

Sept 8: Landsat 7; EO-1 (note a good Quickbird collect on the previous day)

Good collect
Reasonable weather, but hot & humid so somewhat hazy
Only corner marker tarps deployed
Recorded ancillary data on spots usually covered by Stennis & MTF tarps
Ground ASD Reflectance Uniformity of: 5.4 % 450-1350nm
6.3% 1410-1800nm

14.3% 1940-2470nm

Summer 2003

Landsat 5: 2003 Useable Data Collections

May 30:	'Brookings Site'	Good but very windy (dust at ground level)
Sept 3:	3M	Good
Sept 19:	3M	Very good

Landsat 7: 2003 Useable Data Collections

July 25:	3M	Fair (hot and hazy)
Aug 26:	3M	Good

Summer 2004

Landsat 7: 2004 Useable Data Collections

June 25:	3M	'shoot between clouds' comparison with EO1 Fair+ ("good" for relative quantification) S. Schiller did initial analysis using 'light trapping' model
July 11:	3M	Fair : scattered clouds/ cirrus over site
Sept 29:	3M	Very good

Gain Calculation Summary:
Landsat 5

	2003			
	3-Sep		19-Sep	
	Gain	*variation (1σ)	Gain	*variation (1σ)
L5-B1	1.295	2.1%	1.285	3.6%
L5-B2	0.653	3.2%	0.667	3.8%
L5-B3	0.901	2.2%	0.886	4.3%
L5-B4	1.051	1.9%	1.046	2.1%
L5-B5	7.994	6.7%	7.293	6.6%
L5-B7	13.681	5.6%	13.362	7.3%

L5-Gain is in DN per W/m2 sr μm
*NOTE: Listed variation is image based only

Landsat 7: ETM+ Gains 2002-2004 SDSU

	2002 (U of Arizona Atmospheric Model)						2003		2004	
	20-Jun		22-Jul		8-Sep		26-Aug		29-Sep	
	Gain	*variation (1σ)	Gain	*variation (1σ)	Gain	*variation (1σ)	Gain	*variation (1σ)	Gain	*variation (1σ)
L7-B1	1.09	3.9%	1.22	2.7%	1.35	2.4%	1.172	2.5%	1.292	3.1%
L7-B2	1.03	4.3%	1.18	3.6%	1.31	2.3%	1.093	3.4%	1.218	3.4%
L7-B3	1.3	6.6%	1.49	3.8%	1.66	4.3%	1.407	2.6%	1.619	3.6%
L7-B4	1.47	2.5%	1.54	2.9%	1.5	3.1%	1.475	1.1%	1.455	1.2%
L7-B5	6.84	5.7%	7.05	2.7%	7.07	2.3%	6.86	2.3%	7.285	2.1%
L7-B7	18.84	7.0%	19.86	2.5%	19.91	4.5%	19.18	5.0%	21.49	4.3%

Landsat 7: ancillary data set

	Schiller's trapped light model 25-Jun-04	
	Gain	*variation (1σ)
L7-B1	*1.184*	*3.0%*
L7-B2	*1.153*	*2.6%*
L7-B3	*1.461*	*2.2%*
L7-B4	*1.402*	*2.1%*
L7-B5	*7.507*	*1.7%*
L7-B7	*22*	*3.0%*

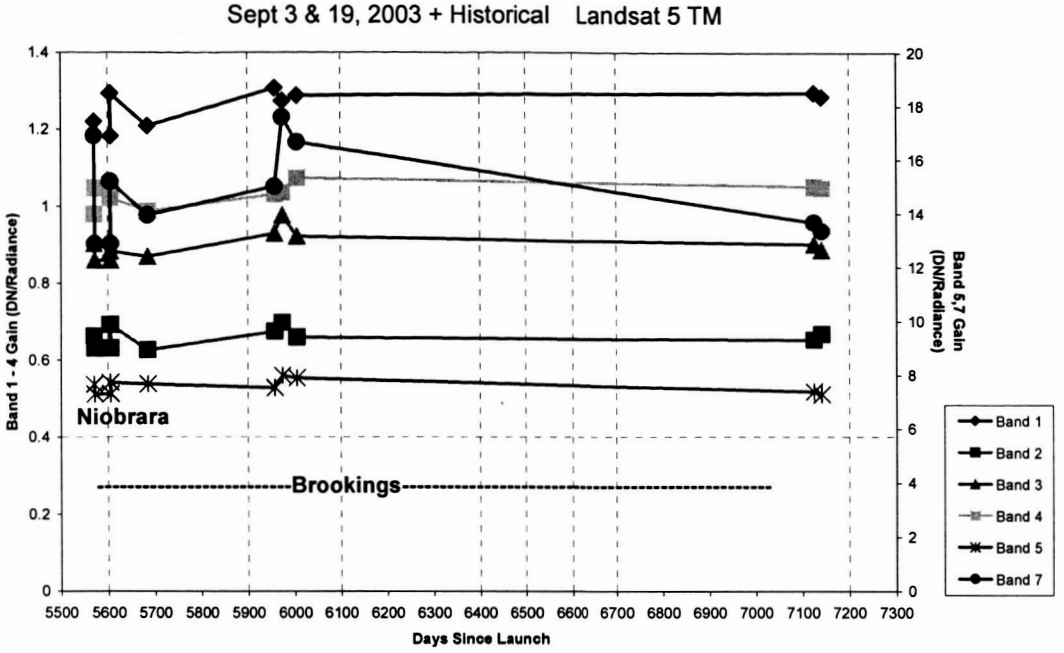

Figure 4: This graph shows the trending for the Landsat 5 TM as measured and evaluated by the South Dakota State University group.

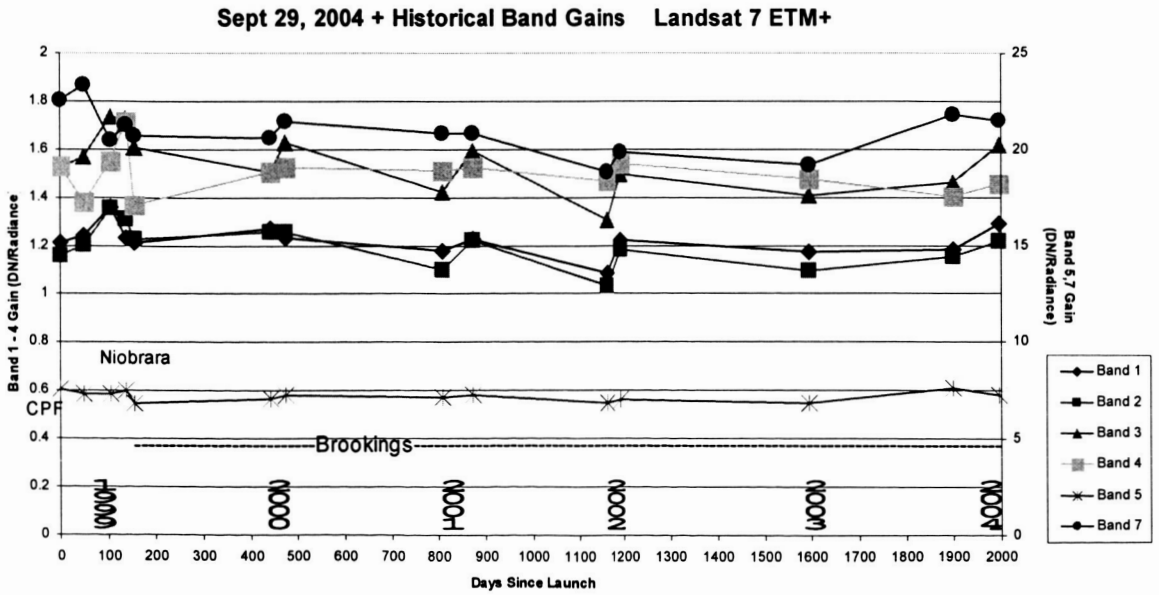

Figure 4: This graph shows the trending for the Landsat 5 TM as measured and evaluated by the South Dakota State University group.

Conclusions:

The trending for both the TM and the ETM+ sensor systems are consistent with previous calibration activities. No change in the present gain coefficients is warranted.

Data acquisition and analysis techniques at South Dakota State University have been fully restored and procedures are now streamlined to improve turnaround time and to make the process more robust.

In conjunction with continued data collection and analysis for the grass site, two additional tasks have been initiated. The first task will be to develop a formal assessment of experimental uncertainty for the SDSU data collection/analysis. The second task is the refinement of a formal algorithm for data analysis in the presence of scattered cloud cover. This will include implementation of the data sorting algorithm mentioned previously and in continuing development of a 'light trapping' model to accommodate the changes in diffuse radiance due to scattered clouds reflecting upwelling radiance.

Relative Gain Characterization

1.1 Background

Relative Radiometric Gain (RG) refers to the phenomenon that occurs whenever an imaging system has more than one detector. With multiple detectors, the responsivity of each detector is slightly different from its neighbors, and possibly every other detector in the array. A model that is often used is

$$DN = g_i * r + b_i \quad (1)$$

where DN refers to the digital number recorded in the image, g_i is the gain of the ith detector (in DN/radiance), r is the radiance incident on the detector, and b_i is the bias of the ith detector (expressed in units of DN). Thus, if a number of detectors are exposed to a uniform radiance level, r, the response will not be uniform. As a result, significant striping visually exists in the imagery and is most pronounced in the homogeneous regions. Since the bias is recorded after each scan, it is a known quantity for each detector that can be removed from the equation and only g_i needs to be estimated for each detector [1].

In this document, a new methodology to destripe Landsat 5 scenes is discussed. The objective is to develop a definitive characterization of the relative radiometric gain of all reflective channels of the Landsat 5 Thematic Mapper instrument. The goal was to develop quantitative models for each of the detectors/channels in the Thematic Mapper. A scene-based approach is used in order to calculate relative gain for each detector. Relative gain (RG) is calculated as (Detector mean / Scene mean). The scenes used in this analysis were artifact corrected before the relative gain calculations were performed. The relative gain values are then modeled into 0th order or 1st order linear models for all detectors/channels. These statistical models are then applied to all the detectors and are used to correct the scene data. The relative gain correction removes residual striping present in scene data.

1.2 Relative Gain Calculation

The underlying theory behind histogram equalization is that the image data from all detectors should have the same mean and standard deviation if they are exposed to the same radiance source. This realization gives the foundation for balancing the radiometric response of each detector [2]. The following development forms the basis for RG correction by histogram equalization. Assume DN_1 and DN_2 are the digital output values of two detectors, detector 2 being the reference detector.

Then

$$DN_1 = g_1 r + b_1 \text{ and } DN_2 = g_2 r + b_2 \quad (2)$$

If both detectors observe the same radiance, then the output DN values should be equal. Substituting for radiance from the first equation into the second yields

$$DN_2 = (g_2/g_1)x(DN_1 - b_1) + b_2 \quad (3)$$

which is the relationship used to normalize the output of detector 1 to the reference detector. The mean value from each detector is

$$DN_{1mean} = r_{mean} g_1 + b_1 \quad \text{and} \quad DN_{2mean} = r_{mean} g_2 + b_2 \quad (4)$$

It can also be shown that the ratio of the gains is equal to the ratio of the standard deviations [2],

$$\sigma_1/\sigma_2 = g_1/g_2 \tag{5}$$

Thus, to implement relative gain correction via histogram equalization, the ratio of standard deviations is substituted into (3) and, in the case of Landsat TM, bias is estimated from the calibration file associated with each scene. However, since bias is accurately estimated from the calibration file, another approach exists to determine the ratio of relative gains. Consider first removing the detector bias to obtain a net DN value as follows:

$$\begin{aligned} DN_1' &= DN_1 - b_1 = g_1 r \\ \text{and } DN_2' &= DN_2 - b_2 = g_2 r \end{aligned} \tag{6}$$

Then the means of the net DN value are simply

$$DN'_{1mean} = g_1 r_{mean} \quad \text{and} \quad DN'_{2mean} = g_2 r_{mean}$$

which leads to

$$g_1/g_2 = DN'_{1mean}/DN'_{2mean} .$$

Thus, the gain ratio can also be calculated from the ratio of means of the net DN values. The lifetime relative gain characterization was implemented using this method where the reference detector was the mean of all detectors (i.e. the scene mean). This approach was felt to be less sensitive to noise since first moments are used rather than second moments.

1.3 RG Characterization

Before computing the relative gain at a scene level for individual detectors, the unprocessed Level 0 (L0R) data were subject to Scan-Correlated Shift (SCS) and Memory Effect (ME) artifact corrections [3] using the processing system implemented at South Dakota State University. Detector bias on a line-by-line basis was calculated from the artifact-corrected calibration data through averaging over a 550-pixel window in the shutter region; these bias values were then subtracted from the artifact-corrected image data. Because Memory Effect had been corrected previous to this step, the bias estimate should be accurate for the entire scan [4].

The calculation of detector and overall scene means used in the relative gain estimates relied on a restriction of image data to values between 5 DN and 245 DN. This was done in an attempt to remove from consideration 'saturated' data and/or potential negative radiance values due to bias error. Although no explicit cloud mask was used, the restricted DN range tended to remove clouds and shadows, which helped in stabilizing the analysis.

From the detector and scene statistics for each scene, the relative gains for each detector were calculated. These time series were used to develop linear gain models for each detector as follows:

- The relative values were first plotted versus time in units of days since launch (DSL), as shown in the example of Figure 1.
- The data points were then subjected to outlier detection. Those with values outside the range of $g_{meani}(t) \pm 2*\sigma$ were considered as outliers (where $g_{meani}(t)$ is

the relative gain value of the ith detector and σ is the standard deviation of the corresponding data values).

- First order linear functions of the form $g_i(t) = A_{1i} \cdot t + A_{2i}$ (where A_{1i} and A_{2i} are the slope and intercepts of the ith detector) were fit to the data.

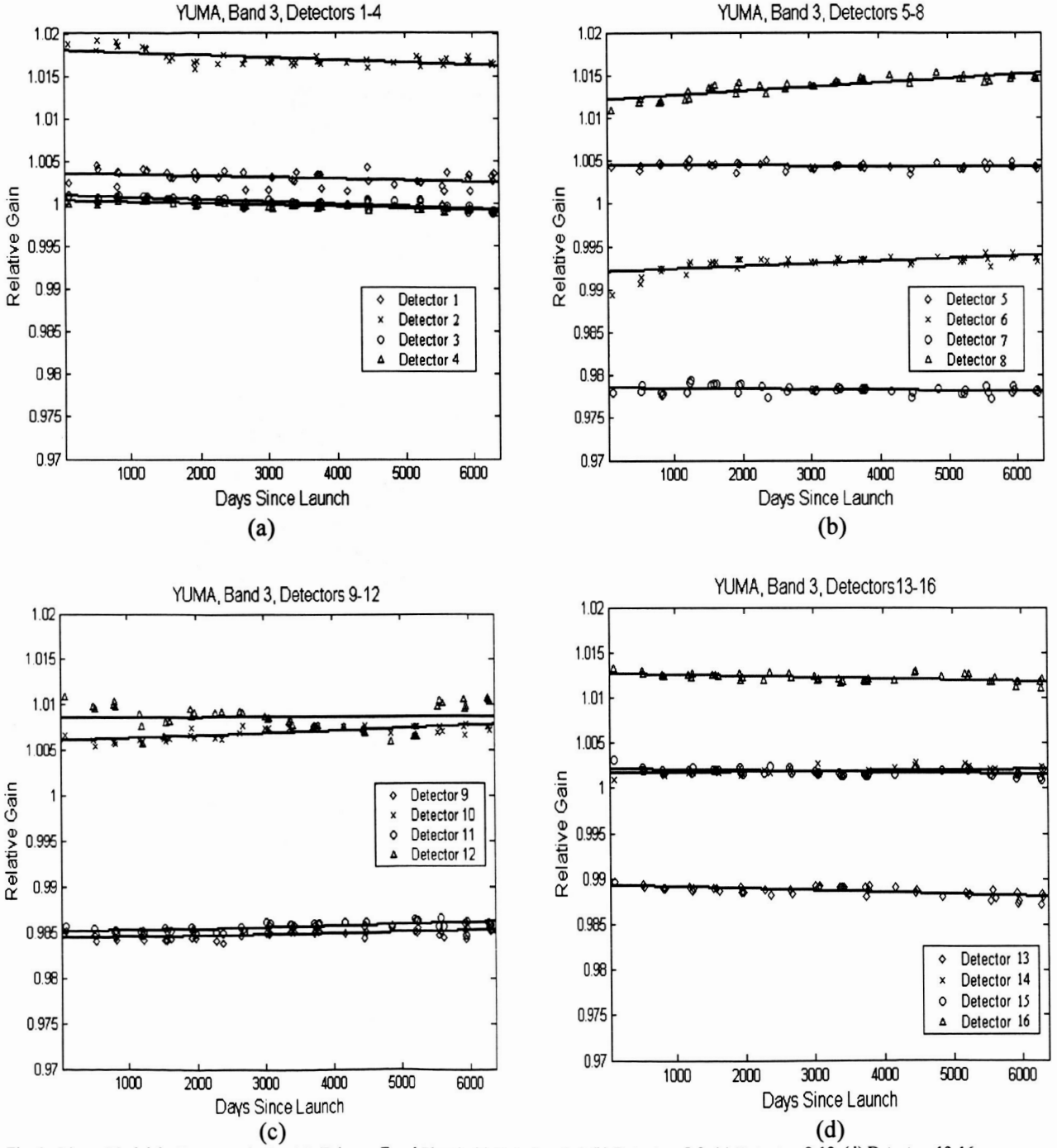

Fig. 1. Linear Model for Detectors in Band 3 (Primary Focal Plane). (a) Detectors 1-4. (b) Detectors 5-8. (c) Detectors 9-12. (d) Detectors 13-16.

1.4 Validation of Relative Gain Models

Three scenes of the White Sands, NM test site (WRS path 33, row 37) acquired May 11, 1986, April 20, 1990, and June 1, 1998 were chosen for correction using the proposed relative gain models. Each validation scene was processed in the same manner as the scenes used in the modeling procedure. The scenes were then corrected using date-specific relative gains predicted from the models. For purposes of comparison, the scenes were also corrected using standard histogram equalization. Figures 2a, 3a, 4a show a 400x400 pixel area extracted from the common subregion for each scene. In these images, striping is clearly evident. Figures 2b, 3b, 4b show the same area after correction with relative gains estimated from the lifetime models, and Figure 2c, 3c, 4c show the same area corrected with histogram equalization. All images have been identically stretched before and after correction to emphasize potential changes resulting from the correction. In general, the images corrected with relative gains derived from the lifetime models show less evidence of residual striping than do the images corrected with histogram equalization.

To provide a quantitative estimate of the degree of residual striping present after correction, an 'integrated' striping metric was calculated for a 400 x 400 pixel homogeneous area within the common subregions before and after correction:

$$SM = \left(\frac{ISR_{before} - ISR_{after}}{ISR_{before}} \right) \times 100\% \tag{7}$$

The ISR terms in (7) represent an 'integrated' striping ratio, defined as the mean striping ratio of all 'significant' components found at multiples of the fundamental frequency of 1/16 cycles per pixel (up to and including the Nyquist frequency):

$$ISR = \frac{1}{N} \sum_{n=0}^{N-1} SR_n \tag{8a}$$

The striping ratio components are estimated from the image subregion, and are defined as the ratio of the average Fourier transform magnitude in the along-track (across-scan) direction to the average Fourier transform magnitude in the cross-track (along-scan) direction [5]:

$$SR_n = \frac{\overline{|F(v_n)|}}{\overline{|F(u_n)|}} \tag{8b}$$

An example striping ratio spectrum before and after relative gain correction is shown in Figure 5. Tables I through VI show the estimated ISR before correction, after relative gain correction, and after histogram equalization; lower values indicate a greater degree of correction. Overall, differences between the two methods tend to be fairly small. Performance of the new approach was better in the primary focal plane bands than in the cold focal plane bands, consistent with the adequacy of the modeling. However, implementation of the relative gain approach simply involves use of a lookup table, whereas histogram equalization requires calculation of image statistics.

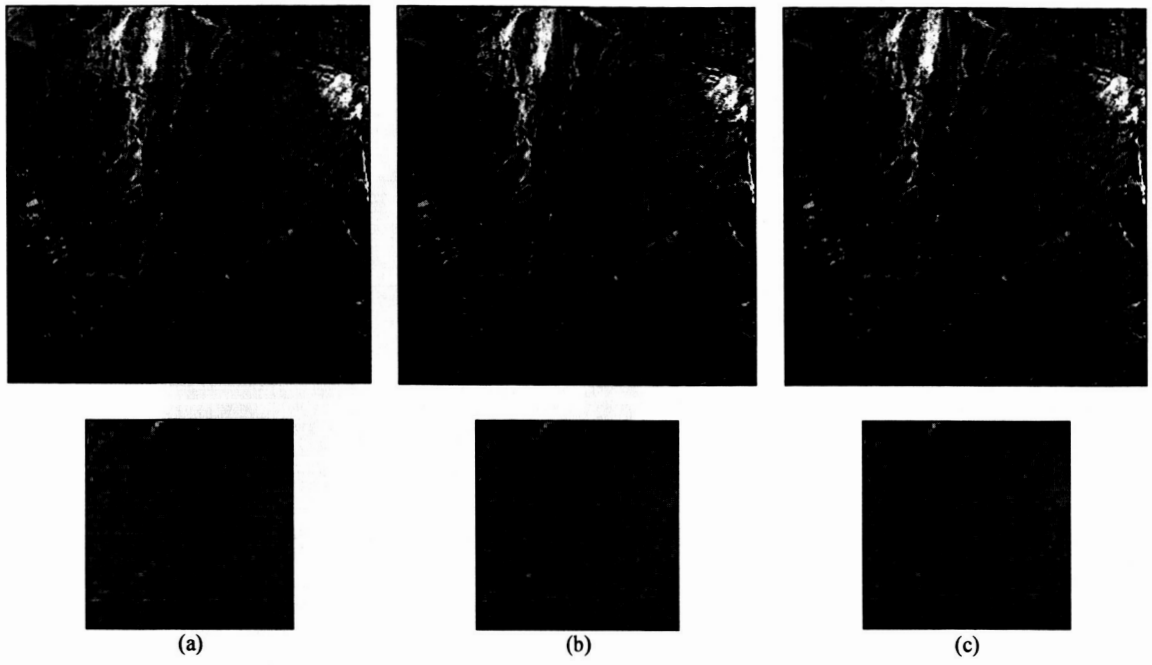

Fig. 2. WhiteSands Scene (May 1986) – Band 3 (a) Before. (b) After RG Adjust. (c) After Histogram Equalization

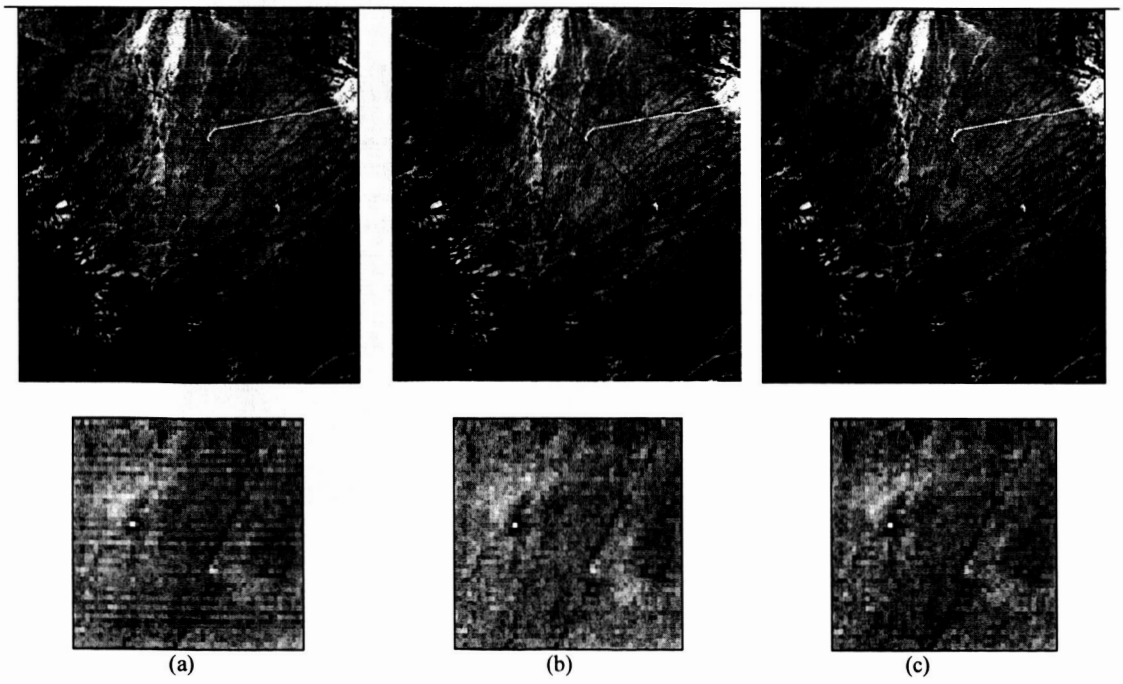

Fig.3. WhiteSands Scene (April 1990) – Band 3 (a) Before. (b) After RG Adjust. (c) After Histogram Equalization.

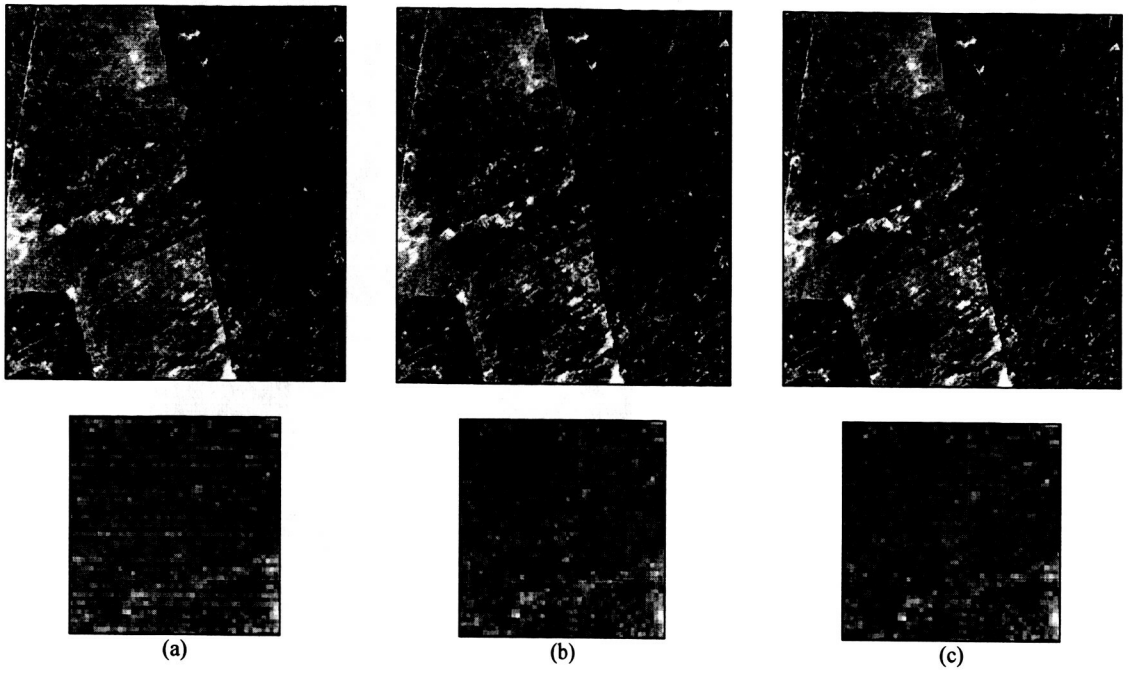

Fig.4. WhiteSands Scene (June 1998) – Band 3 (a) Before. (b) After RG Adjust. (c) After Histogram Equalization

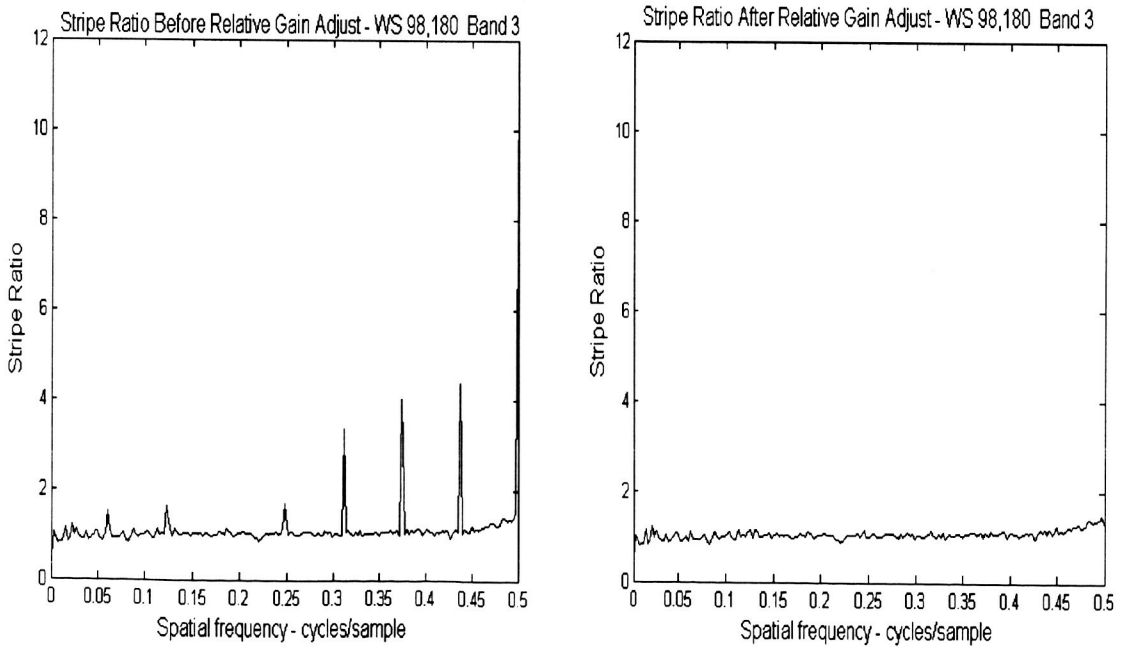

Fig.5. Striping Ratio of WhiteSands Scene (June 1998) – Band 3 (a) Before RG Adjust. (b) After RG Adjust.

TABLE I
ISR ESTIMATES FOR BAND 1

Scene Location/Date	ISR Before	ISR After RG Adjust	ISR After Hist. Eq.	SM	
				RG adjust	Hist. Eq.
WS – 86,131	6.001	0.013	0.272	99.778	95.469
WS – 90,110	5.436	0.277	0.098	94.901	98.197
WS – 98,180	8.839	1.691	2.375	80.865	73.131

TABLE II
ISR ESTIMATES FOR BAND 2

Scene Location/Date	ISR Before	ISR After RG Adjust	ISR After Hist. Eq.	SM	
				RG adjust	Hist. Eq.
WS – 86,131	4.769	0.341	0.382	92.852	91.987
WS – 90,110	2.352	0.175	0.221	92.574	90.626
WS – 98,180	8.262	2.049	1.782	75.196	78.432

TABLE III
ISR ESTIMATES FOR BAND 3

Scene Location/Date	ISR Before	ISR After RG Adjust	ISR After Hist. Eq.	SM	
				RG adjust	Hist. Eq.
WS – 86,131	12.990	0.899	1.030	93.078	92.069
WS – 90,110	13.492	1.458	1.340	89.191	90.063
WS – 98,180	21.161	0.639	2.273	96.983	89.256

TABLE IV
ISR ESTIMATES FOR BAND 4

Scene Location/Date	ISR Before	ISR After RG Adjust	ISR After Hist. Eq.	SM	
				RG adjust	Hist. Eq.
WS – 86,131	4.4475	0.6664	0.4922	85.016	88.933
WS – 90,110	4.8312	1.0436	0.7458	78.399	84.562
WS – 98,180	9.6472	2.9768	1.9643	69.143	79.638

TABLE V
ISR ESTIMATES FOR BAND 5

Scene Location/Date	ISR Before	ISR After RG Adjust	ISR After Hist. Eq.	SM	
				RG adjust	Hist. Eq.
WS – 86,131	7.223	0.551	0.166	92.369	97.701
WS – 90,110	7.001	0.976	0.424	86.064	93.950
WS – 98,180	21.748	2.488	1.177	88.559	94.590

TABLE VI
ISR ESTIMATES FOR BAND 7

Scene Location/Date	ISR Before	ISR After RG Adjust	ISR After Hist. Eq.	SM	
				RG adjust	Hist. Eq.
WS – 86,131	7.115	0.575	0.034	91.921	99.525
WS – 90,110	6.202	0.802	0.131	87.072	97.882
WS – 98,180	6.658	2.138	1.885	67.884	71.684

1.5 Conclusions

The analyses presented in this report demonstrate the stability of the Landsat 5 Thematic Mapper over a 20-year period of continuous operation. Relative gain differences between detectors vary from approximately 0.97 to 1.02. These gains, with a few exceptions, have either been constant or slowly varying over the lifetime. Those detectors that have changed slightly have done so in a manner that allows characterization through fitting of simple linear models. However, detector 1 in Band 7 could not be properly characterized through a linear model. These results have led to an improved method of relative gain correction that is based only on the date that the image is acquired instead of scene content. The RG method is also computationally much simpler than traditional histogram equalization.

However, there are detectors in bands 5 and 7 that have a noisier response thereby decreasing the modeling accuracy. Hence, this would impact the degree of relative gain correction that could be achieved when applied to the scene data. Quantitative results of Band 4 suggest that histogram equalization always tended to produce a higher degree of correction over the suggested lifetime approach. Based on the quantitative results shown, it can be concluded that the lifetime model approach produced a higher degree of correction approaching 75% to 99.7% in Bands 1, 2, and 3. For Bands 4, 5, and 7, application of the same approach results in removal of 67% to 92% of striping. With this approach, relative gain correction can be more accurately performed and overall radiometric fidelity of image data acquired by Landsat 5 Thematic Mapper can be preserved.

1.6 References

[1] D.L.Helder, T.Ruggles, J.Dewald, S.Madhavan, "Landsat 5 Radiometric stability" *IEEE Transactions on Geoscience and Remote Sensing*, pp. 2730- 2746, December 2004

[2] Schowengerdt, R.A. – "Remote Sensing, Models and Methods for Image Processing," pg 301, second edition, Academic Press, 1997.

[3] Helder, D.L., Ruggles, T.A. "Landsat TM Radiometric Artifacts," *IEEE Transactions on Geoscience and Remote Sensing*, pp. 2704-2716, December 2004.

[4] D. Helder, W. Boncyk, R. Morfitt, "Landsat TM Memory Effect Characterization and Correction," Canadian Journal of Remote Sensing, Vol. 23, No. 4, December, 1997, pp. 299-308.

[5] Personal communication with Dr. Dennis Helder, South Dakota State University, Brookings, SD 57007.

Outgassing

Problem description

An artifact, commonly known as Outgassing plagues the radiometric responsivity of the TM Cold Focal Plane (CFP) bands. Detector responses to Internal Calibrator (IC) pulses in Landsat 5 are observed to fluctuate in a cyclic manner about 4.5% in Band 5, and about 3.5 % in Band 7, and exponentially decay in Band 6 over single outgassing cycles – periods between two outgassing events – throughout the instrument's lifetime. Figure 1 represents an example of Bands 5 and 7 detector responses observed during an outgassing cycle in 1987. The attenuation in detector responsivity is removed and every detector's performance regained whenever an outgassing procedure – warming the housing of the CFP detectors from its normal operating temperature of –181° C to the temperature of the primary focal plane (approximately 23°C) followed by cooling down with the purpose to remove potential contaminants within the CFP optics – is performed. Thus, it is postulated that a thin film of some material is deposited on the window surfaces of the CFP dewar much like frost builds up on automobile windshields during winter weather.

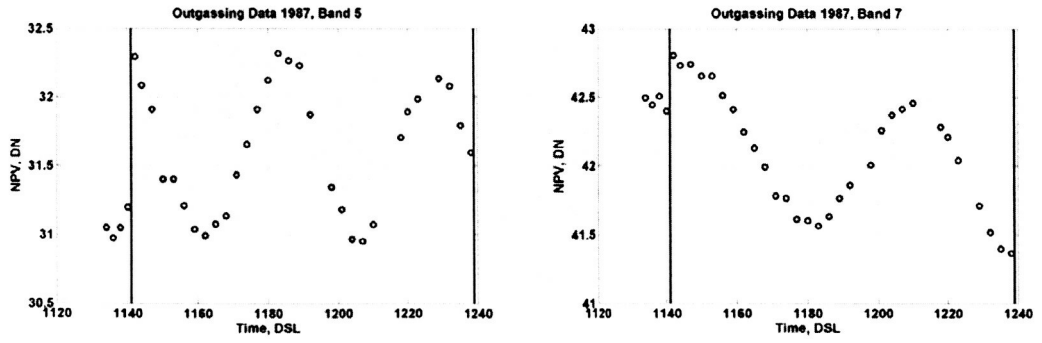

Fig. 1. Bands 5 and 7 detector responses observed during an outgassing cycle in 1987

Theory

Two-film interference model is developed to simulate the cyclic pattern present in the mid-infrared detector responses of Landsat 5 TM. This model is able to predict Band 5 and 7 responses at any point in time simply by knowing when the last outgassing event occurred.

The two-film model layout representing the contaminated ZnSe CFP dewar window is depicted in Figure 2. An antireflective coating (ARC) deposited on the ZnSe substrate to increase transmittance through the window is included in this model as the first thin film layer. The second layer represents the unknown contaminant. An electromagnetic wave incident on such a structure is partly reflected at each of the boundaries, *I*, *II*, and *III*. Additionally, the wave is reflected backward and forward between the interfaces. Multiple reflected waves combine with the incident waves in a process of interference.

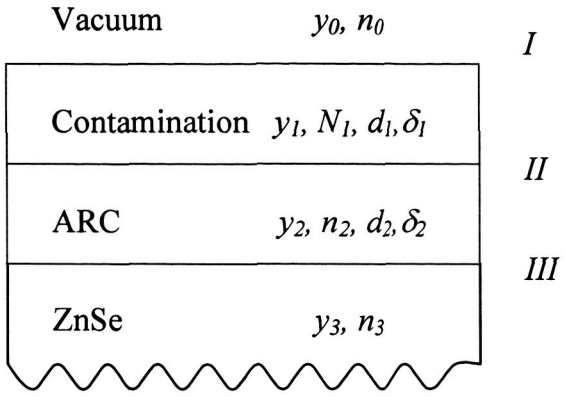

Fig. 2. Two-film model layout. The boundaries between layers are labeled with Roman numerals. The ZnSe layer represents the dewar window material.

The mathematical treatment used to derive expressions for electric and magnetic fields at the interfaces is based on an application of Maxwell equations at the interfacial boundaries. For a normally incident electromagnetic wave at interface *I*, the electric (*E*) and magnetic (*H*) fields on the corresponding boundaries *I*, *II*, and *III* are related as:

$$\begin{bmatrix} E_I \\ H_I \end{bmatrix} = \begin{bmatrix} \cos\delta_1 & j\dfrac{\sin\delta_1}{y_1} \\ jy_1\sin\delta_1 & \cos\delta_1 \end{bmatrix} \cdot \begin{bmatrix} E_{II} \\ y_2 E_{II} \end{bmatrix} = M_1 \begin{bmatrix} E_{II} \\ y_2 E_{II} \end{bmatrix} \tag{1}$$

$$\begin{bmatrix} E_{II} \\ H_{II} \end{bmatrix} = \begin{bmatrix} \cos\delta_2 & j\dfrac{\sin\delta_2}{y_2} \\ jy_2\sin\delta_2 & \cos\delta_2 \end{bmatrix} \cdot \begin{bmatrix} E_{III} \\ y_3 E_{III} \end{bmatrix} = M_2 \begin{bmatrix} E_{III} \\ y_3 E_{III} \end{bmatrix} \tag{2}$$

where M_1 is the characteristic matrix of the film buildup that has the complex index of refraction $N_1 = n_1 - jk_1$ having real index of refraction n_1 and imaginary part, k_1, that accounts for absorption by film material (index of absorption), and the characteristic

admittance $y_1 = N_1 Y_0$, where $Y_0 = 1/377$ Siemens is the admittance of free space. M_2 is the characteristic matrix of the ARC that has the characteristic admittance $y_2 = n_2 Y_0$ and is assumed to have a real index of refraction n_2, and y_3 is the characteristic admittance of the ZnSe substrate in which the absorption is neglected (n_3 is real). The phase difference due to wave propagation through the film build up is given by:

$$\delta_1 = \frac{2\pi N_1 d_1}{\lambda} = \frac{2\pi (n_1 - jk_1) d_1}{\lambda} \tag{3}$$

and the phase difference that occurs when the wave traverses the ARC is:

$$\delta_2 = \frac{2\pi n_2 d_2}{\lambda} \tag{4}$$

where d_1 and d_2 stand for the thickness of the contamination and ARC layers, respectively, and λ is the operating wavelength.

The relation among the fields on the interfaces *III* and *I* is then:

$$\begin{bmatrix} E_I \\ H_I \end{bmatrix} = M_1 \begin{bmatrix} E_{II} \\ y_2 E_{II} \end{bmatrix} = M_1 M_2 \begin{bmatrix} E_{III} \\ y_3 E_{III} \end{bmatrix} = M \begin{bmatrix} E_{III} \\ y_3 E_{III} \end{bmatrix} \tag{5}$$

where M is the characteristic matrix of the two-film model:

$$M = \begin{bmatrix} \cos\delta_1 \cos\delta_2 - \frac{y_2}{y_1} \sin\delta_1 \sin\delta_2 & j\frac{1}{y_2} \sin\delta_2 \cos\delta_1 + j\frac{1}{y_1} \sin\delta_1 \cos\delta_2 \\ jy_1 \sin\delta_1 \cos\delta_2 + jy_2 \cos\delta_1 \sin\delta_2 & -\frac{y_1}{y_2} \sin\delta_1 \sin\delta_2 + \cos\delta_1 \cos\delta_2 \end{bmatrix} \tag{6}$$

After normalizing to the electrical field at the rear interface, E_{III}, the fraction of the irradiance, T, transmitted to the ZnSe substrate can be derived from boundary conditions as:

$$T = \frac{4 y_0 \, \mathrm{Re}(y_3)}{(y_0 E_{In} + H_{In})(y_0 E_{In} + H_{In})^*} \tag{7}$$

where E_{In} and H_{In} are the normalized electric and magnetic fields at the front interface, respectively and '*' represents the complex-conjugate operation. Once the fraction of the transmitted power is determined, it has to be multiplied by a scaling factor specific for a given IC Lamp State (LS), *Sf*, to predict the detector responses, DN:

$$DN = Sf \times T \tag{8}$$

Outgassing Modeling

Four independent, closely-sampled scene sets representing outgassing cycles in years 1985, 1987, 1993, and 1999 have been acquired and the average Net-Integrated Pulse Values (NPV) in Digital Numbers (DN) derived from odd numbered detector responses to the second strongest IC lamp (LS 010) during reverse scans. The two-film model parameters are estimated based on analysis of each cycle separately in order to achieve consistent model parameter values and, thus, to allow usage of the model for lifetime characterization.

The contamination material, as well as the other media employed in modeling of interference effects on the CFP, was assumed to be linear, homogenous, isotropic, and nondispersive across the bands. Furthermore, the operating wavelengths are assumed to be equal to the corresponding band center wavelengths. That is: 1650 nm for Band 5 and 2215 nm for Band 7. The refractive index of vacuum (free space) is known and equal to 1 for all wavelengths. The refractive index of Zinc-Selenide is also known and equal to 2.45 for Band 5 and 2.44 for Band 7. The other model parameters have to be estimated using a nonlinear curve fitting technique. One of the keys to success in such a process, which is by nature an iterative one, is to define sufficiently good starting parameter values.

The thickness of the film buildup has to be expressed as a function of time. From the nature of the interference phenomenon, it is known that the optical thickness of the film buildup, $n_1 d_1$, increases for $\lambda/2$ in a time period between two consecutive local minima of transmitted energy. This explains the different periods of oscillations in Band 5 and 7 responses (Figure 1). This also means that there is a direct relationship between the film growth rate and the periodicity of the detector responses. In order to characterize changes in period over the lifetime, the initial periods were estimated by minimum-squared-error fitting of exponentially attenuated cosine curves to the outgassing data sets. The oscillation period was not found to change significantly between the 1985 and 1987 data sets. Later in life (post-1987), a reasonably linear increase of period (and a consequent decrease of the film buildup rate) was indicated in both bands, which can be expressed as a function of DSL:

$$T_p(t) = mt + b \tag{9}$$

where m and b are the slope and intercept, respectively, of a regression line fitted to the estimated oscillation periods, and t is the time since launch in DSL. Thus, the initial parameter values for m and b in Band 5 are 0.03968 and -4.823, and in Band 7 0.06167 and -20.62.

The film thickness will increase during a given period, T_p, by:

$$d_f = \frac{\lambda}{2n_1} \tag{10}$$

The film buildup rate, r_b, in nm/day is the ratio between the given film thickness d_f and the time needed for its deposition and, is given by:

$$r_b(t) = \frac{d_f}{T_p} = \frac{\lambda}{2n_1 T_p} \tag{11}$$

for the early lifetime (T_p constant), and

$$r_b(t) = \frac{d_f}{T_p(t)} = \frac{\lambda/2n_1}{mt + b} \tag{12}$$

for the later lifetime, taking into account the time dependence given by (9).

The film thickness, $d_1(t)$, accumulated since an outgassing event occurred on day t_{OG} can be determined by integrating the expression for the film build-up rate. For the early lifetime that is:

$$d_1(t) = \frac{\lambda}{2n_1 T_p}(t - t_{OG}) \tag{13}$$

and later in life:

$$d_1(t) = \frac{\lambda}{2n_1 m} \ln\left(\frac{mt + b}{mt_{OG} + b}\right) \tag{14}$$

The contaminating film material is not known, but there is some evidence that it could be ice or an ice mixture that forms by condensing water vapor on the Cold Focal Plane window. The wavelength dependent complex refractive index of ice for the center wavelength of Band 5 (1650 nm) is 1.2878-j0.000241, and for the center wavelength of Band 7 (2215 nm) it is about 1.2608-j0.000232.

Information about the structure of the ARC used for coating of the CFP ZnSe windows in Landsat TM was not available. For that reason, the initial values of the *effective* thickness and refractive index were estimated according to general ARC design principles—zero reflectance is achieved when the ARC has an index of refraction equal to the geometric mean of the refractive indices of the adjacent media, and an optical thickness (product of the thickness and the index of refraction) equal to an odd multiple of one quarter of the operating wavelength—and with regard to the band center wavelengths. Then, the initial values for Band 5 are $n_{ARC} = \sqrt{n_0 n_{ZnSe}} = \sqrt{1 \cdot 2.45} = 1.565$ and $d_2 = 263.6\,\text{nm}$, and for Band 7 $n_2 = 1.562$ and $d_2 = 354.5\,\text{nm}$.

The value for the scaling factor, S_f, used in Equation (3.8) needs to be close to the average detector responses in DN since the transmittance, T, is always close to 1. Then,

the appropriate initial values for LS 010 would be in the range of 32 – 35.5 for Band 5 and 42.5 – 47.5 for Band 7.

The final parameter values for each single outgassing data set were estimated based on a least-squares error criterion that is optimized using the Nelder-Mead downhill simplex algorithm. There were many sets of parameters for each outgassing data set that provided very similar solutions using a least-squares error criterion. Therefore, as additional condition, the final parameter set is to be chosen such that the contaminant's index of refraction is closest to the index for ice.

In order to extend procedures used in modeling of single outgassing cycles to the whole instrument's lifetime, the outgassing data sets had to be corrected (normalized) for the apparent increase in overall Band 5 and 7 detector responses after approximately 1600 DSL due to changes in IC lamp outputs. The correction for this 'lamp effect' (LE) is illustrated in Figure 3. First, mean values for each data set were calculated from the responses acquired during the time between the outgassing procedure and the following maximum, and a quadratic function, f_{LT}, was defined such that it passed through those mean values. The 1993 and 1999 data sets were then normalized to the 1987 data through multiplication by a correction factor, C_{LT}, defined as:

$$C_{LT}(DSL) = \frac{M_{87}}{f_{LT}(DSL)} \tag{15}$$

where M_{87} is the mean DN value of the first cycle in 1987 response data. After the LE correction, the variability in Band 5 and 7 data is assumed to be only due to outgassing effects

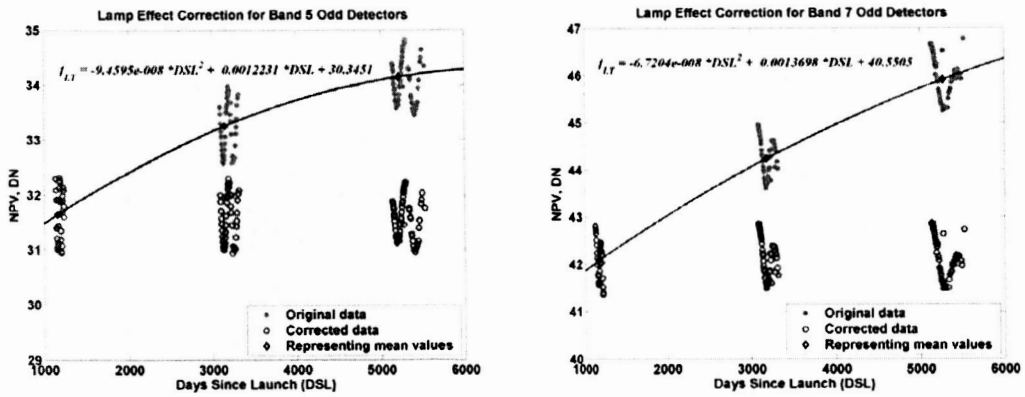

Fig. 3. LE correction function f_{LT} applied to Band 5 and Band 7 NPV data

Fitting the two-film model to detector response data from individual outgassing cycles resulted in slightly different parameter sets for each cycle. As the oscillatory pattern in the Band 5 and 7 responses is assumed to be caused by accumulation of the

same contaminant over the whole lifetime, model parameters for each outgassing cycle should remain constant. To find a unique parameter set applicable over the entire lifetime, a full lifetime model (LM) was constructed using all available individual data sets, with the oscillation period remaining constant early in life and allowed to increase later in life. DSL 1434 was chosen as the approximate date when the oscillation period began to increase, as it corresponds to the date imaging was resumed after outgassing procedure #18. The date when the detector responses start to increase due to changes in lamp output is also not precisely known. For the purposes of this analysis, DSL 1630 was chosen as the last date prior to its onset.

Modeling results

Final parameter estimates derived for each individual outgassing data set and for the lifetime model fitted to all single cycle data sets together are shown in Tables I and II for Bands 5 and 7, respectively. The resulting Band 5 and Band 7 LM fits are shown in Fig. 4. In the lower four plots, the upper curve represents the original data, and the lower curve is the LE corrected data with the model fit. The overall mean squared error (MSE) of the lifetime model indicates that a better lifetime fit was obtained for Band 7. This is primarily due to the poorer fit in the early lifetime for Band 5. Not surprisingly, this is the time interval with the shortest oscillation period in general. In addition, the Band 5 oscillation period is even shorter than the corresponding Band 7 period, thus it will be more sensitive to parameter estimation errors.

Table I: Estimated Model Parameter Values Derived from Nonlinear Fits to the Single Outgassing Data Sets and LE-Corrected Lifetime Model (LM), Band 5

Parameter	**1985**	**1987**	**1993 (reduced)**	**1999**	**LM**
n_1	1.2878	1.2881	1.2879	1.2891	1.2878
k_1	0.0008793	0.0001660	0.00006549	0.001087	0.0007258
n_2	1.683	1.6420	1.6759	1.6849	1.6739
d_2, *nm*	272.1	257.5	272.2	269.4	269.0
m	-	-	0.04091	0.04188	0.03876
b	-	-	-5.73	-14.93	-0.94
T_p, *days*	43.70	44.16	-	-	45.75
S_f	32.382	32.326	34.018	35.065	32.41
MSE	0.003376	0.005704	0.006552	0.001838	0.01787

Table II: Estimated Model Parameter Values Derived from Nonlinear Fits to the Single Outgassing Data Sets and LE-Corrected Lifetime Model (LM), Band 7.

Parameter	1985	1987	1993 (reduced)	1999	LM
n_1	1.2608	1.2606	1.2603	1.2606	1.2606
k_1	0.001768	0.001646	0.001530	0.002493	0.002472
n_2	1.6733	1.6789	1.6658	1.6633	1.6677
d_2, *nm*	326.5	311.9	326.3	331.5	326.9
m	-	-	0.06221	0.06207	0.06224
b	-	-	-20.93	-7.319	-18.59
T_p, *days*	64.09	63.44	-	-	68.54
S_f	42.923	42.977	45.1036	46.8801	43.015
MSE	0.002616	0.001795	0.01386	0.003350	0.01111

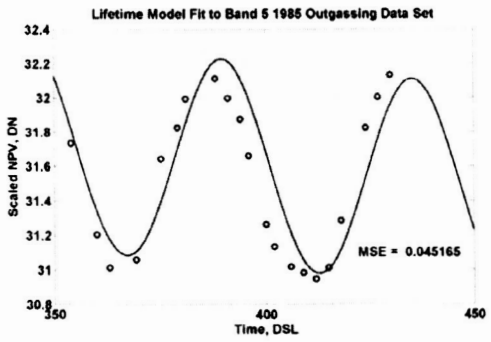

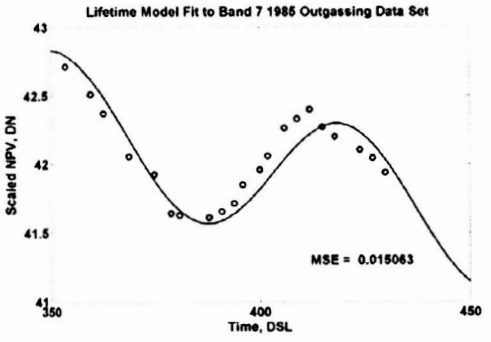

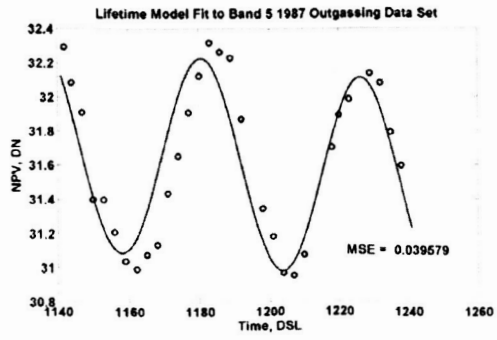

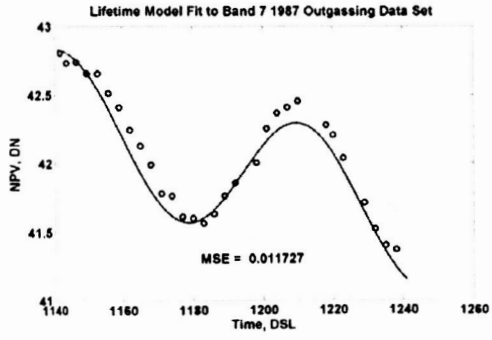

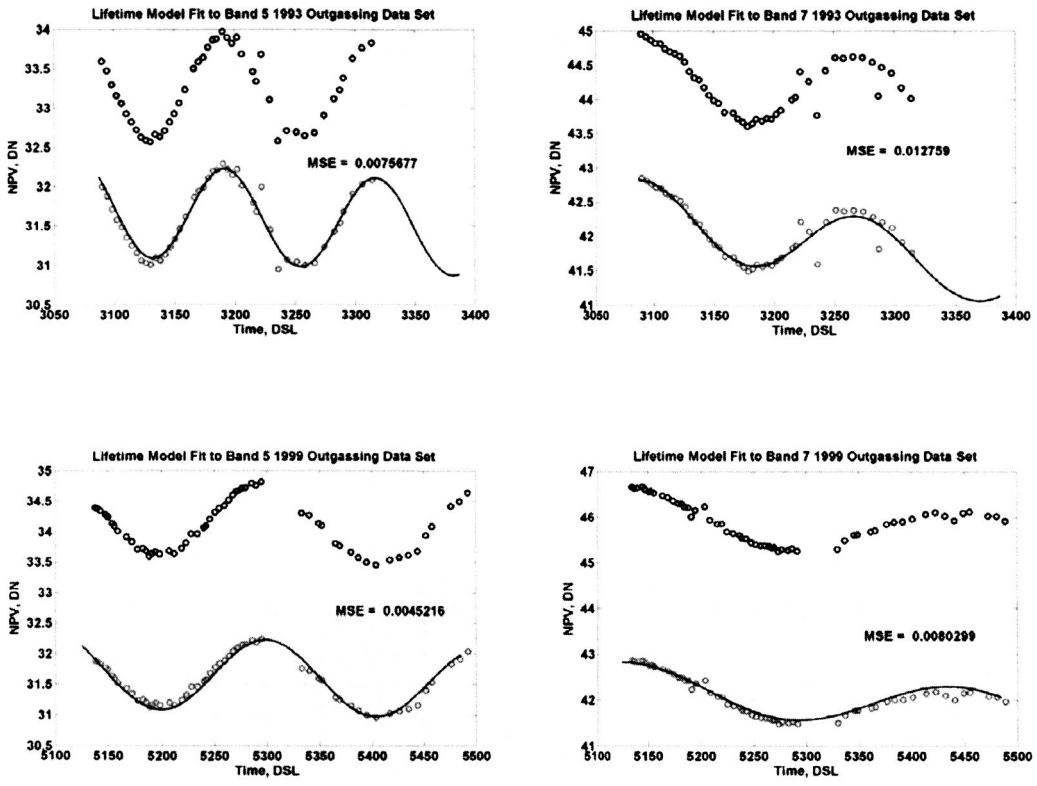

Fig. 4. Lifetime Model fits to individual outgassing data sets. The 1993 and 1999 data sets were corrected for LE prior to modeling (bottom curves and data points). In all cases, the MSE values are associated with the models.

It is evident from the Tables I and II that the estimates for the effective optical properties of the ARC obtained from both models agree among all the data sets, with the exception of the 1987 data set; the difference is greater in Band 5. The ARC optical thickness can then be used to account for phase shifts present in detector response (provided that complete contaminant removal occurs during an outgassing procedure, and that the dates of outgassing procedures are accurately known). The different phase observed in the 1987 data set could be explained as a change in the ARC composition (e.g. deterioration of one or more layers in a multilayered structure), or by incomplete removal of the ice film during the outgassing procedure; however, the 1987 data set appears to represent the most complete outgassing procedure, as the detector response data start closest to a maximum. Differences in the absorption factor k_I of the film thickness can be considered as a random error in modeling, because the estimation of its relatively small value is limited by the accuracy of the observed IPVs.

The slope, m, which characterizes change in oscillation period is found to be a very unstable parameter in each single cycle data set. It may change its sign with a very small change in the starting value of another parameter; this is usually followed by an abrupt change of the intercept b. This indicates that the change in period of oscillation that occurs during an OG cycle is so small that it is difficult to estimate well. Assuming that the amount of available film material decreases in an OG event (e.g. through a valve), there is a possibility that the period does not change at all during OG cycles. In that case, the observed change in period over the instrument lifetime could be explained as a step-wise change occurring after OG processes.

Correction for Outgassing effects

The DN value extracted from the lifetime model for the day of any outgassing event gives the detector response DN_0, when no ice is accumulated on the CFP (32.1 DN for Band 5 and 42,83 DN for Band 7, when odd detector responses to IC lamp [010] analyzed). The DN value corrected for outgassing effects, DN_{cor}, for any detector response DN can be determined as:

$$DN_{cor} = DN \times \frac{DN_0}{DN_{010}} = DN \times \frac{Sf \times T_0}{Sf \times T} = DN \times \frac{T_0}{T} \qquad (16)$$

where DN_{010} is Net Integrated Pulse Value derived from odd numbered detector responses to IC lamp [010] at a given DSL, T_0 is the fraction of the EM radiation transmitted through the CFP without an ice layer, and T is the transmittance extracted from the LM for a given DSL.

The 91-scene SCS-corrected lifetime data set was used to test the corrections produced by the lifetime model. Results of the correction applied to the data set for Bands 5 and 7 are shown in Figure 5. From this figure, relatively good correction can be observed in both bands, with the exception of the early life period and the time interval during 1993 and 1994. Overall, the analysis results indicated that the variation from the estimated DN_0 value after correction was reduced 68% in Band 5 and 77% in Band 7 over the instrument lifetime after DSL 175, excluding the time interval during 1993 and 1994 from consideration. Band 7 responses tended to be better characterized due to a longer oscillation period and consequent decreased sensitivity to phase shift effects.

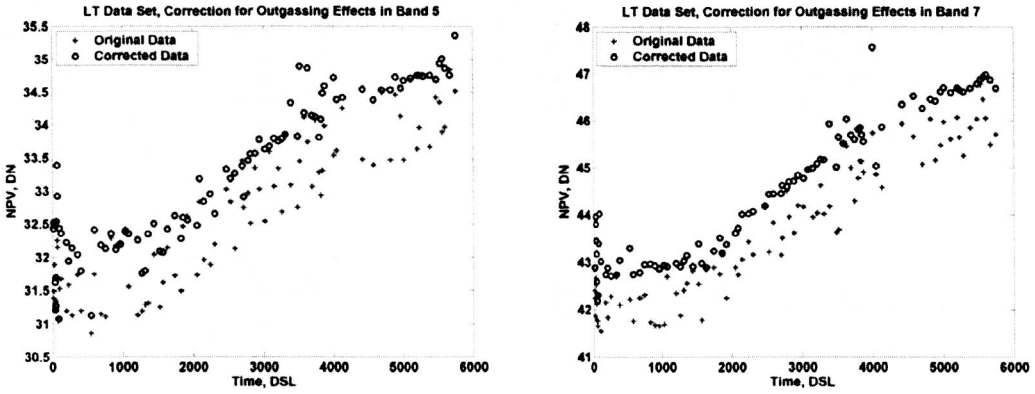

Fig. 5. Lifetime Model correction applied to the Band 5 and Band 7 lifetime test data sets.

Summary

The correction for outgassing effects has been implemented for the Band 5 and 7 absolute calibration lookup tables used by the National Landsat Archive Processing System (NLAPS) at the EROS Data Center. General application of this correction can potentially improve Band 5 and 7 calibration accuracy to levels consistent with the accuracy of the primary focal plane bands, on the order of 5%.

Landsat 4 Absolute Calibration

A complete characterization and calibration was attempted for Landsat 4's Thematic Mapper. This entailed analyzing the Internal Calibrator (IC) to verify the system was stable throughout the life of the instrument, applying existing correction models to the data to remove Scan Correlated Shift (SCS) and Memory Effect (ME) artifacts, and determining and applying a Relative Gain (RelGain) model to the data. Then, when the Landsat 4 data was completely corrected, a cross calibration model using Landsat 4 and Landsat 5 geolocated data was determined. Results of the correction effort show that the models significantly improved the Landsat 4 data and the initial result of the cross calibration effort looks very promising.

A relative calibration was performed first using the IC. A data set of 260 scenes was studied. Due to a gap in the data, two models for each reflective band were required. Only the four reflective bands were studied at this point due to lack of an outgassing correction. The data was further restricted to only reverse scans, to stay consistent with Landsat 5's IC study, and data from the primary lampstates [001], [010], and [100]. Once the data were selected and processed, the lamp data was recorded. This record included readings from each detector, in every band in the PFP, for lampstates [001], [010], and [100].

The goal of the IC lifetime analysis was to determine a single model for each band in the PFP. However, to arrive at this model, the lifetime trends had to be analyzed at multiple lower levels. First, detector trends were studied to verify no single detector was performing differently than the rest. Then 'odd/even' trends were studied. An odd/even trend refers to averaging all odd numbered detectors together and all even detectors together. This is a valid study due to the physical layout of the detectors within a band on the TM instrument. Next, the lampstate trends were studied. This trend is the average of all the detectors within a band, after any necessary corrections were made for odd/even effects, for each of the three lampstates. It was determined that lamp [001] was performing differently than the other two lamps; therefore, it was not included into the final model. Finally, all the data from lampstates [010] and [100] were averaged into band trends and models are determined.

Now the band trends could be studied and lifetime IC models could be determined. It was decided to use two models for each band, one for the pre-gap data and one for the post-gap data because in each band there is a significant difference between the trends after the gap. These models are in the form of a Linear + Exponential regression. This model was chosen because of the work done previously on the Landsat 5 TM. The model coefficients are displayed in Table 1 and the Goodness-of-Fit statistics are shown in Table 2. The RMSE values for each model are very good, less than 0.01 RMSE. The R-squared values are also acceptable. Bands 1 and 4 are quite good, $R^2 > 0.7$, but Bands 2 and 3 are a bit lower, around 0.5.

Table 1: IC lifetime models for Landsat 4 PFP bands $y = ae^{(bx)} + cx + d$

	Coefficients for IC models			
Model	**a**	**b**	**c**	**d**
pre-gap Band 1	0.1190	0.0210	-3.471E-05	1.086
pre-gap Band 2	0	0	2.772E-05	0.984
pre-gap Band 3	0.3250	0.0270	1.449E-05	0.974
pre-gap Band 4	0.0770	0.0120	2.465E-05	0.965
post-gap Band 1	-0.1216	-0.0004	1.384E-04	1.009
post-gap Band 2	-0.0002	-0.0016	4.185E-05	0.931
post-gap Band 3	-4.167E-05	-0.0019	3.737E-05	0.937
post-gap Band 4	-1.863E-05	-0.0020	3.006E-05	0.949

Table 2: Goodness-of-Fit statistics for the IC lifetime models

	Band 1	**Band 2**	**Band 3**	**Band 4**
Pre-Gap R-sq	0.84	0.60	0.57	0.92
Pre-Gap RMSE	0.004	0.004	0.003	0.001
Post-Gap R-sq	0.73	0.66	0.64	0.84
Post-Gap RMSE	0.008	0.007	0.008	0.005

After the IC models were created, the RelGain striping in the image was analyzed, modeled and removed. This effort was largely simplified by referring to the work previously performed on Landsat 5. This method produced a model that considered data spanning the lifetime of the instrument and produced improvements greater than 75%, assuming the scene being improved had some striping already present in the image. If there was no striping present (Striping Ratio before correction < 4) and the scene mean was extremely low (mean < 20), the models failed. In this case, the old method of histogram equalization correction should still be used. However, the number of scenes with both of these restrictions are very few; most of the scenes were improved drastically, many by > 90%. Figure 1 shows an example of RelGain and the results after correction.

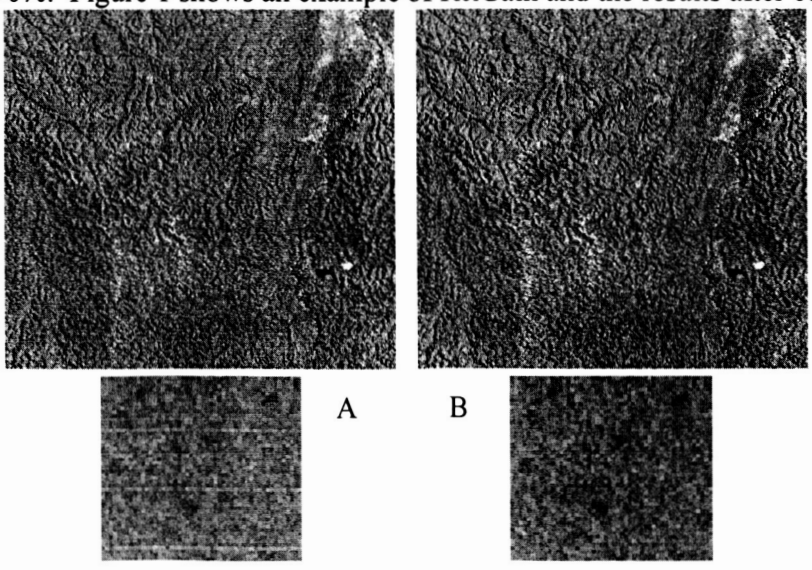

Figure 1: Relative Gain qualitative analysis of Peru B4; Day 267, Year 1988, Path 007, Row 064 **Correction of 96.7%.**
A) Before Correction. B) After Correction.

The last step of this effort was to attempt a radiometric cross calibration (CrossCal) was for the Landsat 4 and 5 TMs. To perform this study, Landsat 4-Landsat 5 scene pairs were obtained and compared. An assumption was made that the ground and atmosphere, and therefore the radiance, did not change during the time between samples. These images were to be homogeneous and near perfectly geolocated. Hence, any difference in the image would be due to the difference in the instruments. This difference could be modeled and then removed from the data. To model these differences, eight small sub-images were chosen throughout each scene-pair studied; unfortunately, only two scene-pairs were obtainable at the time of the study.

Once these pairs had been chosen, data points were calculated by determining the average DN value of a sub-image. The data was analyzed by plotting L5 data on the x-axis and L4 data on the y-axis and a regression line through these points, anchored at the origin, was determined. Also included on these plots are one-to-one lines for reference; if the reference line fell directly on the one-to-one line, no correction would be needed. An example of this is shown in Figure 2 and the gain results are displayed in Table 3. Also in Table 3 are the 1-Sigma values of the residuals and the corresponding percent error. All bands had less than 2% error except band 5.

Table 3: L4/L5 Gain Ratio results for each Band

Band	Gain	1-Sigma Value	Percent Error
Band 1	1.058	2.3	1.7%
Band 2	1.052	1.3	1.8%
Band 3	1.035	1.6	1.6%
Band 4	0.978	1.5	1.4%
Band 5	0.889	6.1	3.3%
Band 7	1.003	1.9	1.7%

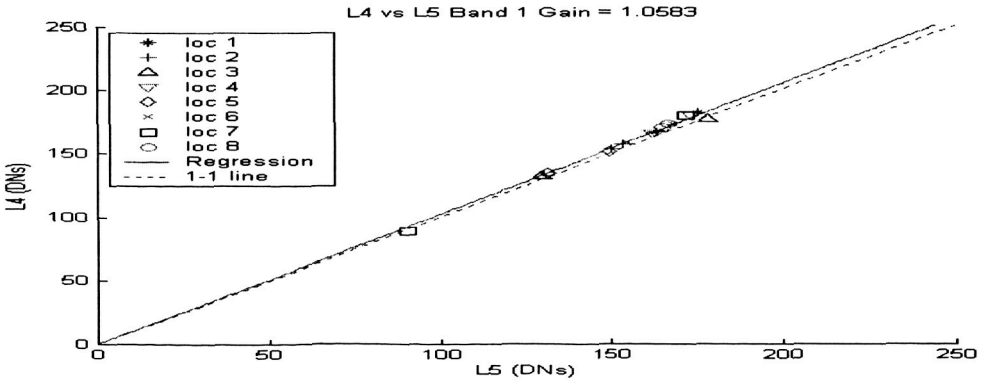

Figure 2: L4/L5 Gain Ratio, Band 1

Band 5 was studied further and it was determined that much of the excess error was due to the outgassing cycle. While, at the time of this study, there was no outgassing model for band 5, the appropriate outgassing cycle had been plotted. By normalizing one data point to the other this error was reduced to 1.7%, which was equal to the average error across the bands.

These models produced CrossCal points on the specific days of the scene pairs. However, a lifetime model was desired. To do this, the IC models were scaled to the CrossCal points, resulting plots are shown below. The blue line is the IC model, the 'x' are the CrossCal points, and the red line is the adjusted calibration model.

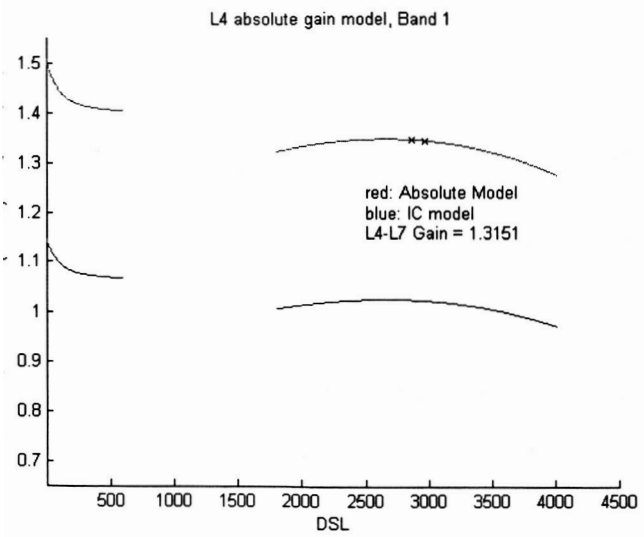

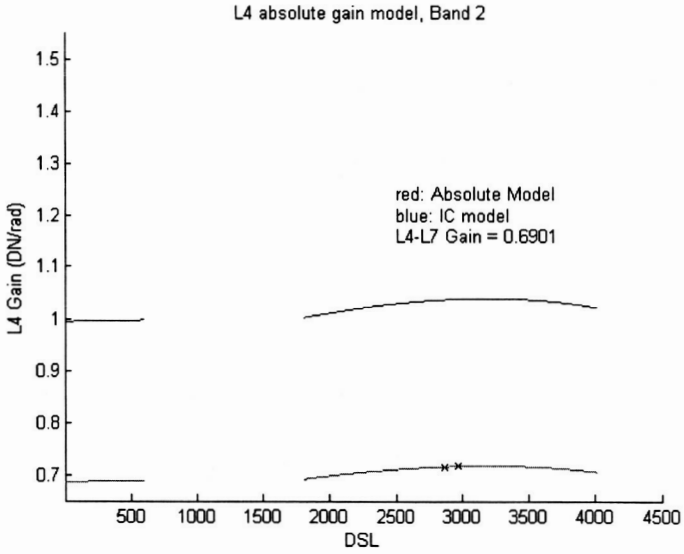

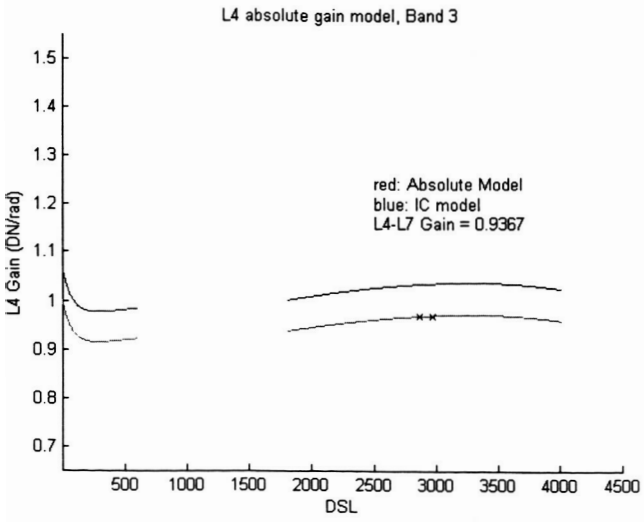

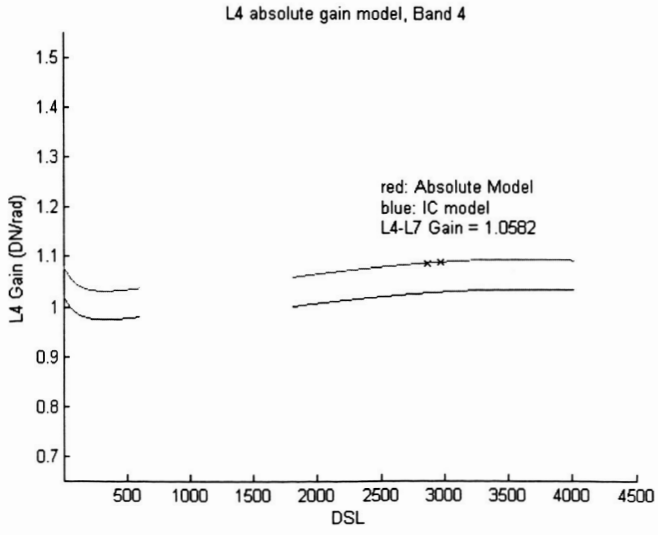

Lastly models for the absolute gain of Landsat 4 were developed. The equation for the model is the standard exponential plus linear equation that was used with Landsat 5 TM:

$$G_{L4} = Ae^{Bt} + Ct + D$$

	Coefficents for L4 Absolute Gain Model			
Model	**A**	**B**	**C**	**D**
pre-gap Band 1	0.1565	0.0210	-4.565E-05	1.428
pre-gap Band 2	0	0	1.913E-05	0.679
pre-gap Band 3	0.3044	0.0270	1.357E-05	0.912
pre-gap Band 4	0.0815	0.0120	2.608E-05	1.021
post-gap Band 1	-0.1599	-0.0004	1.820E-04	1.327
post-gap Band 2	-0.0001	-0.0016	2.888E-05	0.643
post-gap Band 3	-3.903E-05	-0.0019	3.500E-05	0.878
post-gap Band 4	-1.971E-05	-0.0020	3.181E-05	1.004

Summary

A lifetime radiometric model for the absolute gain of Landsat 4 has been developed. The key features of this model are that it is based on use of the IC an interpolator over the lifetime of the instrument. The absolute gain of the instrument was obtained by cross-calibration with Landsat 5 using nearly concurrent scene pairs of invariant sites. A relative gain model was developed for the instrument, as well, to remove striping and radiometric errors due to non-uniform detector gains within a band.

Landsat 5 Scene Invariant Analysis

Introduction

During the 2003 contract year, work was begun on alternative methods to determine/ validate the absolute radiometric gain of the L5 TM sensor (bands 1...5 and 7) via examination of "invariant" sites. Initial results and methodology were reported in the 2003 Annual Report based on processing of Yuma and RRV data sets. The early results indicated a measurable change in sensor response for bands 1 & 2 of approximately -12% and -10% respectively over the initial 6000 days of operation. Effort was expended to incorporate a linear decay term into the accepted IC based gain model to account for effects observed in the scene invariant data. The results were reported at the Calibration meeting hosted at SDSU. During 2004, additional work was undertaken to further process the Yuma data set and enhance the gain model for bands 1 and 2. Results were reported at the Lake Tahoe calibration meeting, and are summarized in this final report.

Results

Efforts were limited to examination of TM bands 1 & 2 where a reasonable amount of sensor responsivity change was observed above the noise level. The primary gain model extension attempted was to fit normalized scene observations with the following empirical model:

$$f(DSL) \equiv \frac{a}{b + [c * \exp(d * (DSL - s))]} + e$$

This model allowed for initial and final state existence, along with an exponential transition between the states. Prior to fitting to the Yuma data set, a Savitzky-Golay filter was applied to smooth the data and account for non-periodic sampling. Results of the SDSU processing effort are presented in Figures 1 and 2.

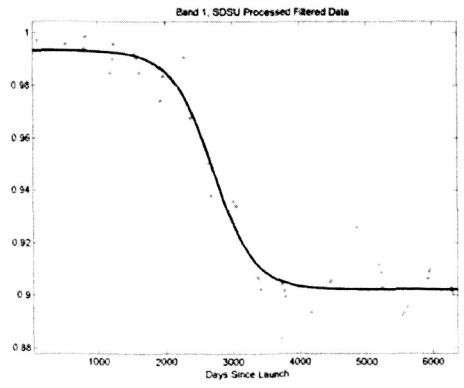

Figure 1: Band 1

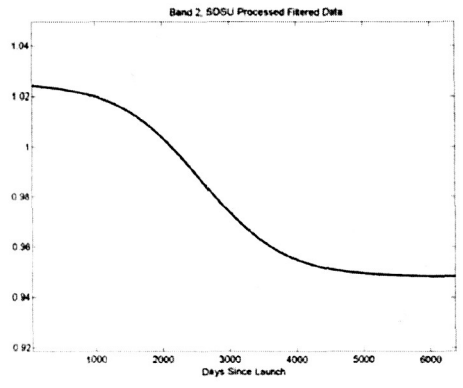

Figure 2: Band 2

While unexplained oscillations are apparent in both Band 1 & 2 data sets, it was decided to denormalize the resulting model, tie the results to the 1999 L7 cross-calibration and

compare to the accepted IC and vicarious gain results. Figures 3 and 4 present the final models that were developed. Shown are two potential scene invariant gain models which differ due to the input data utilized (The curves labeled SDSU Invarient was based on large scene regions, while the curves labeled GSFC Invarient were modeled with small region means provided by Ed Kaita at GSFC).

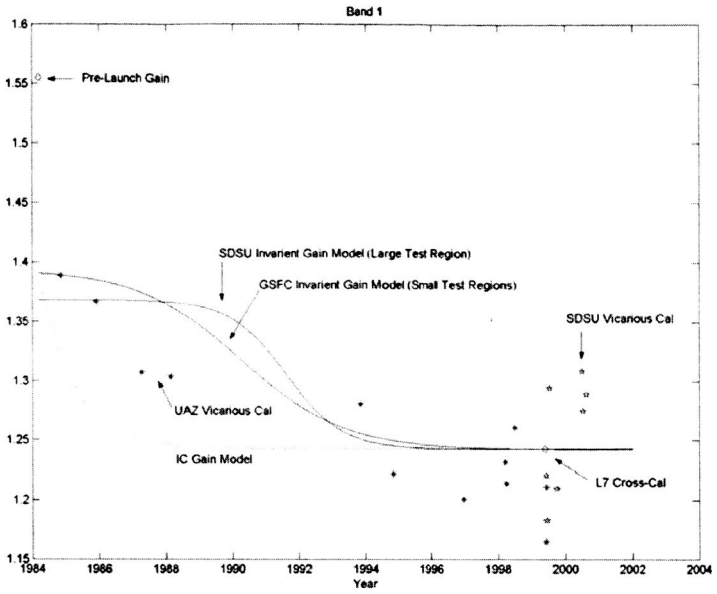

Figure 3: Band 1

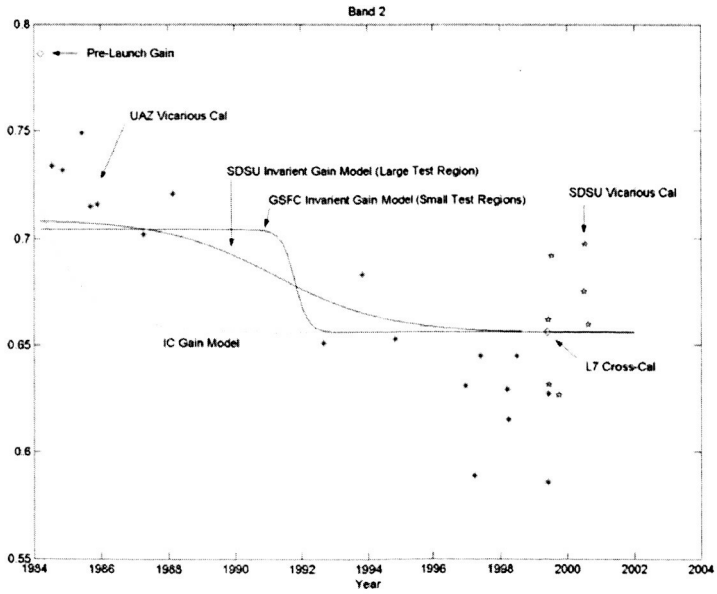

Figure 4: Band 2

Examination of the resulting gain models, in comparison to the IC gain model and vicarious data points, reveals some unexpected results. First and foremost, a significant difference exists in the models wherein the accepted exponential responsivity decay during the early days of the mission is not evident in the Yuma scenes. Secondly, a transition was observed in the Yuma data approximately 3000 days after launch, but not observed in the IC data. The vicarious data does little to resolve the discrepancy, splitting the difference for Band 1 IC and scene invariant models, and indicating a higher gain than either the IC or scene-based models for Band 2. Critical observations during the 1989-92 period which might help to resolve the matter are not available. The end conclusion is that insufficient evidence was provided by the scene invariant approach to justify changing the status quo regarding how DN's are converted to radiance for Level 1 L5TM products. Development of the TMIAS by NCEROS provides an opportunity for further study of both the IC and scene based methods.

SUMMARY

The previous sections have outlined work done in six major categories.

First, the Landsat 5 IC has been extensively studied and trended. The major change that has been observed in the past three years is a significant degradation in the performance of all lamps. It is unlikely that the lamps will be useful after about 2002 for any radiometric trending. Fortunately, the response of the instrument has been stable for 10 years prior to this occurrence suggesting that, although the lamps are failing, there is reason to believe the detectors will remain stable.

The second major area of study is vicarious calibration. The past three years has seen a significant change in personnel and capabilities. After a few years of not being able to perform a full vicarious calibration, the SDSU group is again able to provide absolute gain estimates using ground-based data collection and atmospheric modeling. In addition, an emphasis has been placed on accurate, repeatable data collection, as well as being able to provide calibration estimates in a 'production environment' with a rapid response time. Gain estimates have been comparable with results obtained by other investigation teams.

One of the more troubling aspects of Landsat radiometry has been with respect to the relative gains of detectors within each band. This has historically resulted in a striping pattern on imagery that is not only annoying but a source of radiometric error. Histogram equalization using data from individual scenes has been the heritage method of addressing this problem. A study was undertaken to expand that method using multiple scenes over the lifetime of the instrument to develop a more accurate model of relative gains. This approach relies on the stability of the detectors relative one another as has been borne out on many image examples. Using the results of this study, relative gain correction is as simply as looking up the relative gain of each detector and applying a simple multiplicative factor for correction.

In the cold focal plane, the outgassing effect has continuously plagued radiometric models for Bands 5 and 7. Work under this project has developed a Landsat 5 outgassing model that treats the effect as a thin film phenomenon. Based on this model an accurate and robust correction algorithm has been developed that essentially removes this radiometric error. This technique has been implemented into standard processing at the EROS Data Center.

An absolute gain estimate for Landsat 4 has been developed. It is based on the data collected by two lamps of the IC. These data sets are tied to a cross-calibration with Landsat 5 using a pair of scenes collected at nearly the same time and over the same region. Results from this study indicates a cross-calibration with L5 that is accurate to around 3%. Unfortunately, gaps exist in the L4 data sets and it is difficult to extend this model accurately back to the day of launch. However, it is felt that to date this is the most accurate absolute gain estimate of Landsat 4 available.

The last area of study involved using invariant scenes as an aid in understanding the absolute calibration of Landsat 5. This approach indicated very consistent results with Bands 3-5, and 7. However, Bands 1 and 2 results were different during the earlier portion of the Landsat 5 lifetime. Unfortunately, during the critical part of the lifetime analysis, where a large change is indicated, there is very limited data available to study the effect closely. Thus, initial thoughts are to disregard this approach until more data is available and a more thorough study can be performed.

Lastly, it can clearly be seen that several major contributions to the understanding of the radiometric performance of Landsat 5 have been achieved by this group. This is especially important in light of the recent failure of L7 and the need to continue data into the future.